Optical Nanospectroscopy

Applications

Edited by
Alfred J. Meixner, Monika Fleischer, Dieter P. Kern,
Evgeniya Sheremet, Norman McMillan

DE GRUYTER

Gagik Shmavonyan, Dmitry Cheshev, Andrey Averkiev,
Tuan-Hoang Tran, and Evgeniya Sheremet

5.4 Nanospectroscopy of graphene and two-dimensional atomic materials and hybrid structures

5.4.1 Key messages

- Graphene and other 2D materials are becoming more and more popular thanks to their unique properties in comparison to bulk materials. Graphene has found several commercial applications and along with other 2D materials has enormous potential. The properties of these materials are intensively investigated, in particular by optical spectroscopy methods.
- High-resolution spectroscopic and microscopic techniques allow for the identification and characterization of graphene and 2D atomic materials and their hybrid structures synthesized by conventional (e. g., micromechanical exfoliation, liquid phase exfoliation, chemical exfoliation, chemical vapor deposition (CVD) on metal surfaces, epitaxial growth on electrically insulating surfaces) and nonconventional (e. g., substrates rubbing) methods.
- Raman spectroscopy allows the identification of bonding in 2D materials. Based on a Raman spectrum, the layer thickness of graphene and other 2D materials can be identified easily, fast, and nondestructively. Besides, the presence of defects, strain, and doping of materials can be evaluated based on their Raman spectra.
- Photoluminescence (PL) spectroscopy is one of the widespread optical spectroscopy techniques that allows the characterization of several key properties of materials, for instance, the electronic structure of the materials, their quality, and their purity.
- Tip-enhanced Raman scattering (TERS) takes advantage of a scanning probe microscopy (SPM)-Raman platform combined with surface plasmon resonance effects localized at the tip apex to provide accurate information about the sample with nanometer spatial resolution.

5.4.2 Pre-knowledge

Most conventional materials we deal with in everyday life are 3D. We are now starting to understand how the properties of bulk materials change if one moves to the nanoscale. Layered bulk materials

Author contribution: G. Shmavonyan is the lead author who wrote the major part of the chapter, while D. Cheshev, A. Averkiev, T. H. Tran, and E. Sheremet added the part devoted to optical spectroscopy methods as well as edited the other parts of the chapter.

https://doi.org/10.1515/9783110442908-018

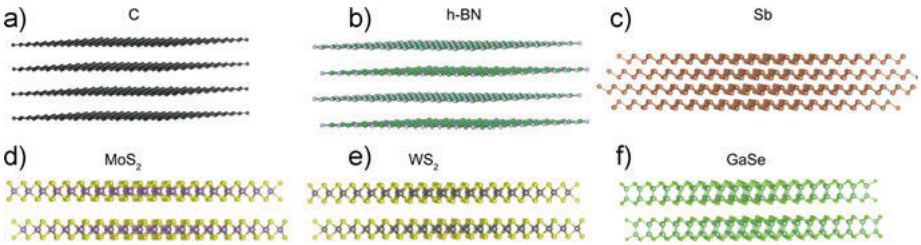

Figure 5.4.1: Crystalline structures of (a) graphene, (b) hexagonal boron nitride, (c) antimony, (d) molybdenum disulfide, (e) tungsten disulfide, and (f) gallium selenide.

exhibit strong in-plane covalent or ionic bonding along two dimensions and weak out-of-plane van der Waals (or hydrogen) bonding. The weak nature of van der Waals bonding (40–70 meV) and surface tension (60–90 mJ/m^2) allow for exfoliating layered bulk materials into 2D atomic materials [1, 2]. 2D materials are divided in three classes: (a) layered van der Waals solids, (b) layered ionic solids, and (c) surface-assisted nonlayered structures (i. e., silicene) [3]. The most studied 2D material is graphene due to its amazing properties. Beyond graphene, there is a wide spectrum of 2D materials, which include 2D layers and layered structures, whose total thicknesses vary from an atomic layer to a few nanometers [4]. The members in the 2D layered materials family are the following: (a) the graphene family (graphene, h-BN, and fluorographene or graphene fluoride [2D carbon sheet of sp^3 hybridized carbons with each carbon atom bound to one fluorine, $(CF)_n$]) [5], BCN compounds (compounds of boron, carbon, and nitrogen atoms), and graphene oxide (compound of carbon, oxygen, and hydrogen atoms), (b) 2D chalcogenides (MoS_2, $MoTe_2$, WS_2, WTe_2, $ZrSe_2$, NBS_2, GaSe, GaTe, InSe, etc.), and (c) 2D oxides (MnO_2, V_2O_5, MoO_3, WO_3, TiO_2, TaO_3, RuO_2, perovskite type $LaNb_2O_7$, etc.). Crystalline structures of some 2D materials are shown in Figure 5.4.1.

A host of 2D layered materials are the transition metal dichalcogenides (TMDCs), transition metal oxides, and nitrides [6]. TMDCs have been known in their bulk form for decades. They are a large class of 2D layered materials with the formula MX_2, where X is a chalcogen (S, Se, Te) and M is a transition metal element from group IV (Ti, Zr, Hf, etc.), V (V, Nb, Ta), or VI (Mo, W, etc.) [7]. The wide range of compositions of 2D layered materials spans the periodic table [6]. Depending on the combination of the atoms of the transition metal and the chalcogen, a variety of TMDCs with properties ranging from semiconducting, metallic, semimetallic, or ferromagnetic to superconducting properties can be obtained [7]. For example, monolayer h-BN and fluorographene are insulators, MoX_2 and WX_2 (i. e., MoS_2, $MoSe_2$, WS_2, WSe_2) are semiconductors with direct band-gaps, and NbX_2 and TaX_2 (i. e., $NbSe_2$, $TaSe_2$) are metals [8]. The band-gaps of monolayer InSe, $MoSe_2$, WSe_2, MoS_2, phosphorene, WS_2, and h-BN at room temperature are equal to ~1.25 eV, ~1.5 eV, ~1.7 eV, ~1.8 eV, ~2.0 eV, ~2.1 eV, and ~5.9 eV, respectively.

There are many 2D atomic materials that go beyond TMDCs, including monochalcogenides (GaSe, GeSe, SiS, etc.) and monoelemental 2D semiconductors (silicene, phosphorene, germanene, etc.) [9]. Silicene is a 2D allotrope of silicon with a hexagonal honeycomb structure (similar to that of graphene) consisting of silicon atomic layers [10]. Contrary to graphene, it is not flat and has a periodically buckled structure. Due to the latter, silicene has a tunable band-gap when applying an external electric field. Phosphorene is a single atomic layer of bulk phosphorus. Germanene is a single atomic layer of germanium, the electronic properties of which are unusual, like those of graphene and silicene. It has no band-gap, but one can be opened by attaching, e. g., a hydrogen atom to each germanium atom.

This chapter will focus on a few 2D materials most studied by optical spectroscopy techniques. It is helpful for the reader to be familiar with the fundamental characteristics of semiconductors (Volume 1, Chapter 1.4), electronic spectroscopy (Volume 1, Chapter 2.2), optical (PL) and vibrational spectroscopy (especially Raman, TERS) (Volume 1, Chapters 2.3 and 3.1), and the basics of materials

for nanotechnology (Volume 2, Chapter 6). Regarding materials and characterization methods at the nanoscale, detailed information on quantum dots and nanocrystals is given in Volume 2, Chapter 6.1, whereas scanning-probe microscopy techniques are discussed in Volume 2, Chapter 4.5.

5.4.3 Importance of the application

The most well-researched and prominent representative of the 2D materials is graphene. This is how an atomically thin sheet or single layer of carbon atoms was named by German chemist Hanns-Peter Boehm in 1962. The term "graphene" was combined from the word "graphite" and the suffix "-ene," which was taken from the end of the word "ethylene." Theoretical research into graphene started in the 1940s and continued for the next decades, boosted from the 1980s by the discoveries of fullerenes (graphene curled up into balls) and carbon nanotubes (graphene folded into a cylinder) [11]. Until 2004, it was theoretically believed that single-layer graphene (SLG) could not exist due to thermodynamic instability when separated under ambient conditions. However, once graphene was isolated by Andre Geim and Konstantin Novoselov working at the University of Manchester, UK, it became clear that it was actually possible. The reason graphene can be obtained is due to very strong carbon-to-carbon bonds in it, which prevent thermal fluctuations from destabilizing it. The researchers applied Scotch tape to peel off layers of highly oriented pyrolytic graphite (HOPG) and obtain multilayer, few-layer, and monolayer graphene flakes. After producing them they successfully identified a single layer of carbon atoms or monolayer graphene flakes from multilayer ones. They published their research in the journal *Science* in 2004 and received the Nobel Prize in physics for the discovery of graphene in 2010 [3, 12]. When first discovered, graphene was an oddity, but now it has shown many record-winning properties, such as the thinnest, strongest, and lightest material, excellent electrical and thermal conductivity, and optical transparency. The extraordinary properties of graphene make it an ideal test bed to probe fundamental problems in physics, as well as lending itself to a wide range of applications in electronics, photonics, energy, sensors, bioapplications, etc. [13, 14].

As outlined in the Pre-knowledge section above, the discovery of graphene gave rise to a new class of atomic materials, known as "2D materials." 2D materials include layers of carbon (graphene), boron (borophene), h-BN ("white graphene"), germanium (germanene), silicon (silicene), phosphorus (phosphorene), tin (stanene), molybdenum disulfide (molybdenite), etc. Most of them could be obtained from layered bulk (3D) materials. Though the latter have been studied for more than 150 years, one only recently began to realize their potential for applications in advanced technologies and consumer products such as flexible thin-film field-effect transistors (FETs), photodetectors, sensors, batteries, supercapacitors, etc. A large number of 2D layered materials, such as TMDCs, are semiconductors with direct and indirect

band-gaps that are tunable by the choice of material or external factors. The characteristics of 2D materials are very different from those of their 3D counterparts [15] and rapidly result in new advancements and applications. Compared to bulk materials, such as silicon, 2D materials exhibit novel properties: (a) their surfaces are naturally passivated without any dangling bonds, which are important for the stacking of different 2D structures, (b) strong light–matter interaction takes place, and, moreover, (c) they can cover a wide electromagnetic spectrum due to their varied electronic properties. Their physical properties are strongly dependent on the number of layers [16]. For example, by decreasing the number of the MoS_2 layers, i. e., from few (two to four) layers to a monolayer, there is a transition from semiconducting to metallic properties or from an indirect band-gap of the bulk layered material to a direct band-gap of the monolayer [17]. Thus, identifying the number of layers and determining their properties is a key issue in studying 2D materials. Besides, other factors, such as strain, doping, defects, impurities, etc., can also drastically change the properties of 2D materials. As will be discussed later, the synthesis method strongly affects these properties, and spectroscopic techniques such as Raman and PL spectroscopy can play a key role. Based on Raman and PL spectra, the materials and number of layers can be fast and easily identified. The effects of strain, doping, and defects can also be evaluated. However, due to the diffraction limit of light, the resolution of Raman and PL is on the order of 1 μm. Therefore, nanospectroscopy approaches are promising in terms of nanocharacterization.

New materials can change the world, like the Iron Age came to replace the Bronze Age, then came concrete, stainless steel, silicon and plastics, and now 2D materials are entering the modern era. 2D materials will bring us to the flatland [18].

5.4.4 State-of-the-art

5.4.4.1 Graphene and 2D atomic materials, their hybrid structures and physical properties

The current chapter focuses on graphene and 2D atomic materials, hybrid structures, and their properties, synthesis, identification, characterization, and application. This chapter is structured as follows. In the first part, we will look at what graphene and 2D atomic materials are and how they were discovered. Then we will consider the types and structures of 2D atomic materials, and the main physical, electrical, and optical properties associated with them. Further we will explore various conventional and nonconventional synthesis methods for obtaining mono- and few-layer (MFL) graphene and 2D atomic materials. The main characterization techniques and identification methods of 2D atomic materials with the focus on Raman spectroscopy, PL, and TERS will then be discussed in the next section. This will be followed by a review

of the 2D hybrid atomic heterostructures. Challenges such as contamination, reliability, reproducibility, and scalability for fabrication of large-area 2D materials and heterostructure devices will be discussed. We shall conclude the chapter by nanoengineering issues of 2D hybrid structures before turning to some important applications in 2D hybrid devices. At the end of the chapter flexible electronics and its prospects will be dealt with.

The most widely known 2D material is graphene. Graphene is the mother element of several carbon allotropes, including graphite, carbon nanotubes, and fullerenes. Graphite, or pencil lead, has been known as a mineral for ~500 years. Graphite has a layered 3D structure, consisting of graphene layers (very weakly held together by van der Waals forces) stacked parallel to each other in a 3D, crystalline, and long-range order. The carbon atoms of each layer of graphite are arranged in a hexagonal lattice with an interval of 0.142 nm, and the distance between atomic planes is 0.345 nm [19]. Graphene is about five orders of magnitude thinner than printing paper and about three million times thinner than 1 mm thick graphite lead in pencil. A graphene sheet is also extremely light at 0.77 mg/m^2, which was calculated from the 0.052 nm^2 area of a hexagonal graphene cell. For comparison purposes, paper is ~100.000 times heavier than a single sheet of graphene. A monolayer of graphene has a high theoretical specific surface area of 2620 $m^2 g^{-1}$ [20].

Graphene has a remarkable energy band structure thanks to its hexagonal crystal structure (Fig. 5.4.2a) [5, 12]. Each carbon atom in a SLG sheet has three in-plane covalent bonds (σ bonds) and one orbital bond perpendicular to the plane (π bond). This structure makes it mechanically strong and flexible. Graphene is therefore used in bullet-proof body armor, fabric, and suits. The π bonds hybridize and form the π and $\pi^\star$ bands (Fig. 5.4.2) that contribute to the remarkable conductivity of graphene. The first Brillouin zone of graphene forms a hexagon with high symmetry points at the center of the first Brillouin zone and two inequivalent points K and K′ in the corners (Fig. 5.4.2b) [21, 22]. The π band corresponds to the valence band and the $\pi^\star$ band is the conduction band [22]. In contrast to almost all solids except for the Dirac-type ones, as the valence and conduction bands in graphene touch in the discrete K, K' points, the bonding–antibonding gap closes at the corners of the Brillouin zone, so there is no band-gap (Fig. 5.4.2b). Thus, monolayer graphene is a semimetal or a zero-band-gap semiconductor [5]. The density-of-states is zero at the Fermi level, which is crossed by electronic bands near the six corners of the Brillouin zone (Fig. 5.4.2b) [5, 21]. The charge carriers (electrons and holes) in graphene are called Dirac fermions, and the six corners of the Brillouin zone are called Dirac points (Fig. 5.4.2b) [5]. The electronic dispersion for graphene at the six corners of the 2D hexagonal Brillouin zone is linear [23]. Due to this linear or conical dispersion near the Dirac points, the charge carriers of graphene have zero effective mass and behave as relativistic particles described by the Dirac equation [24]. Many other outstanding electronic properties of graphene are also the result of linear dispersion or the bonding and antibonding of π orbitals [25, 26].

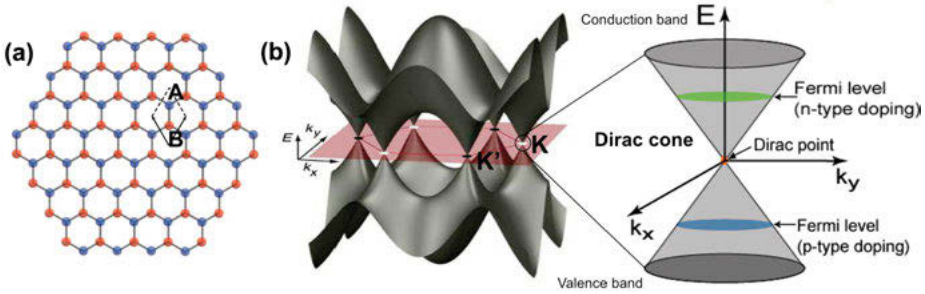

Figure 5.4.2: (a) Hexagonal honeycomb lattice of graphene with two atoms (A and B) per unit cell [27]. (b) Electronic band structure of graphene in the first Brillouin zone and a zoom into one energy band close to the Dirac point. Reprinted (adapted) with permission from Ref. [28]. Copyright 2010 American Chemical Society.

What makes graphene outstanding is that it has the highest known electrical and thermal conductivity. SLG exceeds diamond in electronic mobility (2.5×10^5 $cm^2 \cdot V^{-1} \cdot s^{-1}$) [27, 29] and thermal conductivity (~5000 $Wm^{-1}K^{-1}$, 25 times higher than that of silicon) at room temperature [30]. Graphene also has the highest current density at room temperature (a million times higher than that of copper), it has the highest electronic mobility (200,000 $cm^2 \cdot V^{-1} \cdot s^{-1}$, 100 times more than in silicon), and it conducts electricity in the limit of no electrons (200 times faster than in silicon). However, the limiting factors of the electronic mobility of graphene are the quality of the graphene sheet and the substrate material used. For example, the electronic mobility is limited to 40,000 $cm^2 \cdot V^{-1} \cdot s^{-1}$ in case of monolayer graphene on SiO_2/Si substrate. As electrons in graphene have a longer mean free path (in the order of 65 µm) than in any other material, its charge carriers are able to travel micrometer distances without scattering and operate at ambient temperatures with virtually no resistance. This is similar to superconductivity, but at room temperature. When the mean free path is longer than the dimensions of the material, one can get ballistic transport. The latter is the electron transport in a medium having negligible electrical resistivity caused by scattering. So, graphene exhibits ballistic conduction, the highest electrical conductivity, and the lowest resistivity (10^{-6} Ω·cm, lower than silver).

One of the amazing properties of graphene is its inherent mechanical strength, which is due to its continuous pattern and the strong bonds between the carbon atoms, as each carbon atom in graphene is bound to three other carbon atoms instead of four as in diamond [5]. Due to the mechanical strength of carbon bonds, graphene is the strongest material discovered so far with a Young's modulus of ~1.1 TPa [31] and a high intrinsic strength of 130 GPa (compared to 0.4 GPa for A36 structural steel) [32], which approaches the predicted maximum theoretical value [5]. These strong bonds between the carbon atoms of graphene are also mechanically very flexible. Therefore, it is very elastic and able to regain its initial size after strain [33]. As graphene is bendable and stretchable, it can be relatively easily twisted, pulled, and curved to a certain

extent without breaking. One can stretch a graphene sheet to an additional 25 % of its original length without breaking it. Besides, the graphene monolayer is impermeable, with such closely knit carbon atoms that they can work like a fine atomic net, not allowing other material atoms (i. e., helium, hydrogen, etc.) to get through. It can thus act as a very effective surface passivation layer or protective coating for different materials; e. g., monolayer graphene can protect an underlying metal from corrosion, reactions, etc.

Also, it should be noted that graphene is almost completely optically transparent (it transmits ~97.7 % of white light, compared to ~80–90 % for a window glass). The absorption of ~2.3 % of incident visible light is sufficient for one to see a monolayer of graphene by the naked eye on a piece of white paper. This makes it a great candidate for replacing traditional electrodes by transparent and flexible graphene-based electrodes. The developed organic light-emitting diode (OLED) displays [34], which are thinner, bendable, and more energy-efficient than conventional displays, can be applied in e-book readers, smart cards, e-posters, etc. They reflect light like paper, which allows reading more comfortably and provides a wider viewing angle than most light-emitting displays. Inexpensive graphene touch screens or displays can enable cheap, flexible, and rollable portable electronic devices, which will likely appear in the near future [35]. The same properties make it promising for flexible touch screens and electronic skin or artificial retina applications [36].

Furthermore, graphene could enable ultrafast uploads and replace batteries with quickly and long-lasting light-weight rechargeable batteries or supercapacitors due to its large surface area [37]. Medical applications in contact lenses may enable IR vision, smart plasters may reduce the risk of bacterial infection, and neural interfaces may create a direct connection of machines with the human mind [38]. Filtering and absorbing properties can be employed in the desalination of water, treatment of radioactive waste, and cleaning of oil spills by absorbing oil [39].

The most-studied noncarbon 2D material is molybdenum disulfide (MoS_2), which is also obtained from the bulk structure that appears as a mineral molybdenite. Individual MoS_2 layers have a direct band-gap with an enhanced energy of ~1.89 eV. A single monolayer of MoS_2 can absorb 10 % of the incident light with the energies above the band-gap [40]. Moreover, the MoS_2 monolayer has a thermal conductivity of about 35 $Wm^{-1}K^{-1}$, which is about 100 times lower than that of graphene. These distinguished properties give MoS_2 scientific and industrial importance for example for the creation of electronic devices such as transistors, sensors, solar cells, etc. [41]. MoS_2 monolayers are flexible enough, and thin-film FETs retain their electronic properties when bent [42]. They have a stiffness comparable to that of steel and a higher tensile strength than flexible plastics, making them particularly suitable for flexible electronics.

The compound tungsten diselenide (WSe_2) has a hexagonal crystal structure similar to that of MoS_2. Each tungsten atom is covalently bound to six selenium ligands in

a trigonal-prismatic coordination sphere, and each selenium is bound to three tungsten atoms in a pyramidal geometry [43]. Bulk WSe_2 is a semiconductor with an indirect band-gap of ~1.3 eV, while monolayer WSe_2 has a direct band-gap. The layers are stacked on top of each other by van der Waals interactions and can be exfoliated into thin 2D layers. Recent studies have shown that the WSe_2 monolayer nanostructure has a smaller gap (1.7 eV) and exhibits excellent mobility (250 $cm^2V^{-1}s^{-1}$), and a high on/off current ratio (10^8) at room temperature [44], making it very interesting for electronic and optoelectronic devices [17]. For instance, exfoliated monolayer WSe_2 can be used to create a high-performance p-type FET [45].

Hexagonal boron nitride (h-BN), also known as "white graphene," has a structure based on sp^2 covalent bonds similar to graphene. The h-BN monolayers have a layered structure and lattice structure similar to graphene, with a lattice divergence of only about 1.8 %. 2D h-BN has no absorption in the visible range, but in the ultraviolet (UV) region with good PL. h-BN and graphene differ in electrical conductivity. h-BN is a semiconductor with a direct band-gap of ~5.9 eV and a very high breakdown voltage (>0.4 V/nm). h-BN is widely used as an insulator for the production of ultrahigh-permeability 2D heterostructures consisting of various types of 2D semiconductors (e. g., WSe_2, MoS_2, etc.). h-BN is also a promising material for building high-resolution optical microscopes. Polaritons formed on the surface of a crystal constructed from 99 % pure boron isotope make it possible to lower the diffraction limit many times and achieve even units of nanometer resolutions [46].

Gallium selenide (GaSe) is a layered semiconductor in which each individual layer consists of covalently bound stacks of Se ions at the top and bottom and two levels of Ga ions in the middle in the Se-Ga-Ga-Se sequence, which are held together by van der Waals forces. This makes it possible to exfoliate the structure mechanically or by liquid means. The fabricated 2D GaSe flakes have a tunable indirect band-gap of ~2.1 eV. For the monolayer, the experimental mobility value is ~0.6 $cm^2V^{-1}s^{-1}$, consistent with the transport properties of FETs. 2D GaSe monolayers exhibit nonlinear layer-dependent optical properties. GaSe layers could be used for the development of electronic and optoelectronic devices to realize functional FET and photodetector applications [47].

5.4.4.2 Synthesis of 2D atomic materials

Currently there are numerous techniques for obtaining graphene and 2D atomic materials of various dimensions, shapes, and quality. There are two main ways for their mass production: large-scale exfoliation (obtaining graphene from graphite) and large-scale growth (CVD, etc.), which can be classified into two main categories [48], i. e., top-down (e. g., micromechanical [12, 49, 50], liquid phase [51, 52], chemical [53], electrochemical [54], microwave-assisted [55], exfoliation methods) and bottom-up (e. g., CVD on metal surfaces [56, 57], epitaxial growth on electrically insulating surfaces, such as SiC [58]) processes [59]. First, we will focus on the main conventional

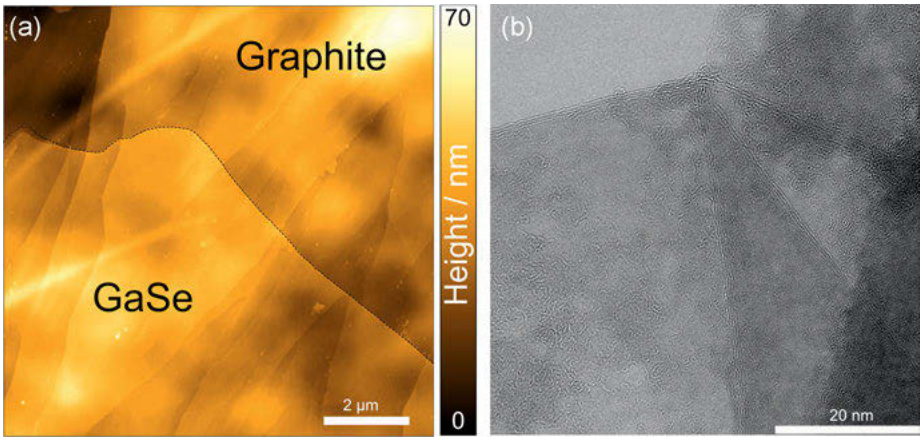

Figure 5.4.3: (a) AFM topography of a GaSe nanoflake on a graphite surface and (b) high-resolution transmission electron microscopy (HR-TEM) image of MFL graphene sheets obtained by the substrates rubbing method. Reprinted (adapted) with permission from [48].

exfoliation and growth methods for obtaining 2D materials and then discuss some nonconventional ones.

Micromechanical exfoliation (Scotch tape method) was used to obtain the first 2D atomic material, graphene, from layered bulk material, graphite, by separation with a Scotch tape. The essence of the method is slicing or multiple exfoliating of layers from the layered bulk material by repeatedly rubbing a piece of graphite against another surface on the Scotch tape until atomically thin flakes are obtained (Fig. 5.4.3b). After that the exfoliated flakes are transferred to a silicon wafer covered with a dielectric SiO_2 layer with a thickness of 300 nm, which allows visualizing graphene flakes through optical interference [12]. Micromechanical exfoliation has been applied to obtain 2D materials such as GaSe (Fig. 5.4.3a), graphene (Fig. 5.4.4a), h-BN, and TMDCs. Though micromechanical exfoliation allows producing high-quality monolayers, it is a nonscalable and time-consuming process with extremely low output and does not allow controlling the flake thickness (atomic layer number) and size (few tens of microns); therefore, its application is limited.

To overcome these problems, the CVD method is used to epitaxially grow large-area and uniform-thickness MFL graphene (Fig. 5.4.4b), MoS_2, GaSe, h-BN, TMDCs, etc., on various substrates, such as SiO_2 or sapphire. As the 2D atomic materials are formed by growing (depositing) layers from gas (vapor), this method is called CVD. The CVD process is based on the decomposition of hydrocarbons on catalytic or metallic surfaces, such as copper, at temperatures above 800 °C [60]. Though CVD synthesis is more scalable than mechanical and chemical exfoliation techniques, there are a few drawbacks. Firstly, they have a higher concentration of structural defects, such as grain boundaries, and it is impossible to avoid the grains. Secondly, it is difficult to control the exact number of atomic layers across a substrate. Thirdly, after the CVD

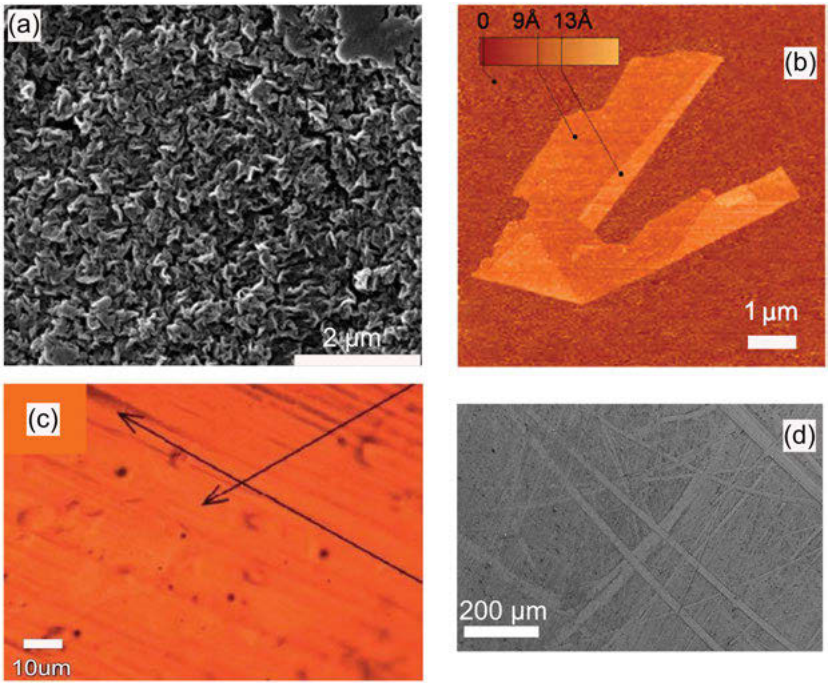

Figure 5.4.4: As-prepared graphene films. (a) AFM image of mechanically exfoliated graphene layers. Reprinted (adapted) with permission from Ref. [78]. (b) Scanning electron microscopy (SEM) image of graphene synthesized by CVD on MgO substrate. Reprinted (adapted) with permission from Ref. [77]. (c) Optical visualization of graphene growth by the CVD method on copper. Reprinted (adapted) with permission from Ref. [79]. (d) SEM image of MFL graphene sheet consisting of nanostripes of quantum dots on silicon substrates obtained by the substrates rubbing method at 1000 rubbing cycles. Reprinted (adapted) with permission from Ref. [48].

epitaxial growth it is necessary to transfer the 2D atomic layer from the catalytic surface to the proper substrate, which is always accompanied by defects. Therefore, until now the reproducible CVD growth of high-quality 2D atomic materials for mass production is still challenging. Another CVD method for producing monolayers is metalorganic CVD (MOCVD), which consists of inserting carbon-based organic gas, such as methane, into a closed container with a metallic film at the bottom and then controlling the temperature and pressure until a monolayer is formed on it. MOCVD growth is realized by chemical reaction and not physical deposition (as in molecular beam epitaxy (MBE)). The possibility to grow graphene by MBE has also been demonstrated [61, 62]. However, the question whether MBE will routinely be used for growing 2D monolayers remains open.

Currently, the simplest, cheapest, and fastest methods for obtaining graphene and other 2D materials are based on the use of graphite-based and raw 2D materials [48] such as mechanical thinning [63], shear exfoliation in liquids [64], hydrothermal exfo-

liation [65], wet ball milling [66], roll-to-roll [67], and arc-discharge [68] methods. This list of the methods can be continued as currently various methods have been proposed to produce 2D materials. Anyway, most of these methods are not industrially scalable ones and cannot be applied for mass production of high-quality and large-size 2D atomic materials. Their up-scaling is still not straightforward due to the difficulty of the setup, the relatively low yield to meet the potential market demand, and usage of different toxic chemicals, solutions, and sophisticated devices [48].

The quality of the synthesized 2D material layers plays a crucial role for the fabrication of 2D devices as the presence of the defects, impurities, grain boundaries, multiple domains, structural disorders, and wrinkles [48] formed in them during growth or post-growth (exfoliation) or the transfer of 2D layers from one substrate (the one it was grown on) to another has an adverse effect on their electronic and optical properties. Depending on the transfer approach, the methods of obtaining 2D materials can be classified as "wet" (i. e., polymethyl methacrylate-assisted transfer (PMMA)) [69] and "dry" (i. e., polydimethylsiloxane (PDMS) stamps) [70]. The problems with wet and dry transfer methods are that (a) polymer or metal residues are resulting on the surfaces of 2D layers and (b) the transfer can increase damage or folding of the 2D atomic layers. For mass production of high quality, preparing large-size and low-cost 2D materials directly on any substrate via cheap, simple, fast, transfer-free, ecologically clean, and universal technologies is important [71]. Industrially scalable nonconventional methods for obtaining high-quality, large-size, and low-cost 2D atomic materials, hybrid structures, and devices directly on any substrate are developed [48, 71, 72].

The author G. Shmavonyan with coworkers proposed the substrates rubbing method [48, 71–74] for obtaining 2D materials (graphene (Fig. 5.4.3b), MoS_2, GaSe, h-BN, etc.), their hybrid structures, dispersion, and powder, which consists of putting pristine bulk (graphite, h-BN, MoS_2, GaSe, etc.) layered material (i. e., crystalline powder) between two solid-state atomically flat substrates or stepped (terraced) surfaces and rubbing the substrates against each other mechanically in any direction, so that the crystalline powder uniformly spreads between them and covers the surfaces of the two substrates with it. It leads to the exfoliation of 2D layers upon multiple rubbings [48, 71–76]. The resulting morphology can be seen in Figure 5.4.4c and d.

The 2D atomic material nanostripes investigated by the author G. Shmavonyan, sheets of nanostripes, and hybrid structures have a unique structure (nanostripes consisting of quantum dots and 2D atomic layers consisting of nanostripes), shape, and size (their length can reach hundreds of meters), advantages which allow to obtain 2D materials of high quality (low-defect and nonoxidized) with clean interfaces (due to a rapid and transfer-free process), achievable from many types of layered material on many solid-state substrates.

After synthesis, the visualization and characterization by spectroscopic methods of 2D atomic materials is important for different applications. Thus, in the following we discuss the application of optical methods for 2D material analysis to evaluate the quality of 2D materials.

5.4.4.3 Identification and characterization techniques of 2D atomic materials

In this section we will consider the prospects and challenges connected with the identification and characterization of 2D atomic materials. There are different characterization techniques for the identification of 2D materials, such as optical, AFM, high-resolution transmission electron microscopy (HR-TEM), scanning tunneling microscopy (STM), Raman spectroscopy, TERS, PL spectroscopy, angle-resolved photoemission (ARPES), and UV-Vis spectroscopy. For more information on these techniques, see also Volume 1, Chapters 2.2, 2.3, and 3.1–3.3 and Volume 2, Chapters 4.5, 6.1, and 6.5. The existing analytical approaches via advanced microscopy tools only exploit the information about the optical contrast of the 2D materials [80, 81]. Meanwhile, the chemical identification of 2D materials and their more detailed characterization require spectroscopy aided by complementary methods such as AFM, which are typically more time consuming. So, there is a growing interest in automating these processes. An artificial intelligence-based approach [82] speeds up the preparation, identification, and characterization of 2D materials, accelerates the discovery of new ones, and predicts properties of materials.

Optical microscopy is an efficient tool for visualizing or identifying MFL flakes from multilayer ones, i. e., graphene from graphite. After obtaining MFL flakes by micromechanical exfoliation, their identification is difficult, but it is an important step for their characterization and application. Under an optical microscope many thick and tiny flakes with different shapes and colors can be observed. Some optical images of as-prepared graphite and graphene flakes obtained on Si/SiO_2 substrate after micromechanical exfoliation are shown in Figure 5.4.5. After the micromechanical exfoliation it is very difficult to find graphene flakes among millions of thicker graphitic ones (Fig. 5.4.5a). For distinguishing monolayers from few-layer or multilayer graphene (bulk graphite) it is necessary to carefully scan the sample surface by an optical microscope, which is a time-consuming process. In case of a SiO_2 layer thickness of 300 nm for interference imaging, the ultrathin flakes have sufficient contrast to differentiate graphene flakes among thicker ones, and thus become visible with an optical microscope. MFL graphene flakes are almost transparent and crystalline shapes, which have darker regions with respect to the substrate (Fig. 5.4.5b). The color of much thicker flakes (more than five layers) does not follow this trend and can change from blue to gray. The SiO_2/Si substrate is the most common one used to visualize MFL. The color of the SiO_2 dielectric layer on the Si wafer depends on an interference effect from reflection of the two SiO_2 layer surfaces. MFL flakes on the dielectric layer modify the interference and create a color contrast between the flake and the substrate. For optimal contrast, the thickness of the dielectric layer needs to be within 5 nm of the ideal value [83]. Visualizing monolayers on other substrates without the need for interference can be done as well. It is possible to directly visualize monolayers (i. e., MoS_2, WS_2) with direct band-gaps by fluorescence microscopy. However, their fluorescence

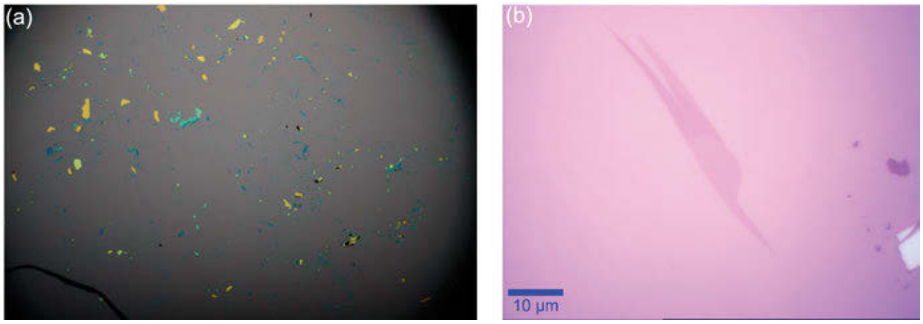

Figure 5.4.5: Optical images with different scales (10× (a) and 100× (b)) of as-prepared MFL graphene and graphite (a) and monolayer graphene (b) on SiO_2/Si substrate obtained after micromechanical exfoliation [84].

reduces as their band-gaps become indirect by increasing the number of the atomic layers.

Raman spectroscopy

After identification of graphene or other 2D material flakes by an optical microscope, they can be precisely distinguished by Raman spectroscopy (cf. Volume 1, Chapter 2.3). The latter is a nondestructive, fast, and powerful characterization technique for characterizing structural properties of 2D materials, such as the number of atomic layers (distinguishing MFL (less than 5 layers)), defect densities, or strain. Raman spectroscopy is an effective method to investigate graphite and its analog. When laser light interacts with a lattice, it induces in-plane or out-of-plane vibrations with single (A, B), double (E), and triple (T) degeneration in the whole lattice, which results in resonance Raman spectra. These vibrations can be longitudinal or transversal with low (acoustic) or high (optical) energy. Let us consider the Raman spectra of graphite and graphene. There are two pronounced peaks in the Raman spectra of high-quality graphene and graphite (Fig. 5.4.6a) [85]. The first peak at a wavenumber of ~1580 cm^{-1} (G peak) corresponds to the in-plane bond-stretching optical vibration of sp^2-hybridized carbon atoms [86]. This vibration in graphene has the E_{2g} symmetry and the G peak is due to the E_{2g} phonon at the Brillouin zone center of graphene [87]. The E_{2g} mode is a doubly degenerate Raman active optical vibration, where the carbon atoms move in the graphene plane [88]. The second peak at a wavenumber of ~2700 cm^{-1} (2D or D′ peak) is due to second-order Raman scattering by in-plane transverse optical phonons near the boundary of the Brillouin zone of graphene [85]. The third peak (D peak) at a wavenumber of ~1360 cm^{-1} is due to the breathing modes of sp^2 atoms and requires a defect for its activation (Fig. 5.4.6b) [89], which makes this method particularly suitable for the confirmation of the material quality. In addition

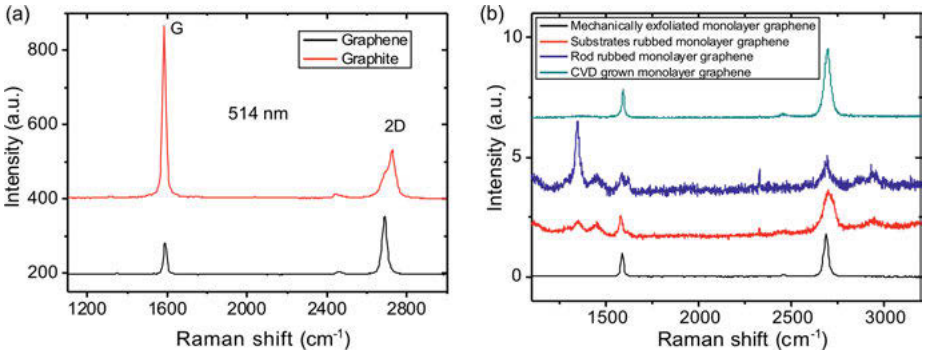

Figure 5.4.6: (a) Raman spectra of monolayer graphene (black) and graphite (red) obtained by micromechanical exfoliation on SiO_2/Si substrate at an excitation wavelength of 514.5 nm [84]. (b) Raman spectra of micromechanically exfoliated (black), substrates-rubbed (red), rod-rubbed (blue), and CVD-grown (gray) monolayer graphene on SiO_2/Si substrates at an excitation wavelength of 514.5 nm. Reprinted (adapted) with permission from Ref. [48].

to the observed intense Raman D, G, and D′ peaks, other, less intense D′ (1620 cm^{-1}), D+D″ (2450 cm^{-1}), and D+D′ (2950 cm^{-1}) peaks are observed [90, 91].

Besides, Raman spectroscopy allows observing new peculiarities of 2D materials. For example, in experiments by Shmavonyan and coworkers, a new peak (with its intensity depending on the number of rubbings) at a wavenumber of 1450 cm^{-1} is observed (Fig. 5.4.6) [48].

The Raman signal of monolayer graphene is easily detectable (Fig. 5.4.6). The obvious difference between the Raman bands of monolayer graphene and graphite is in the second-order D peak, the 2D band. The 2D band of monolayer graphene has a single sharp and symmetric peak, while the same band for graphite consists of four peaks [92]. The line shape of the Raman 2D band of MFL and multilayer graphene is strongly dependent on the number of atomic layers (1 to 4), stacking order, and twist angle between graphene layers. By choosing an appropriate excitation energy, the number and stacking order of atomic layers can be determined. Few-layered graphene has two types of stacking order: Bernal (ABA) and rhombohedral (ABC). Bilayer graphene has a much broader and up-shifted (bathochromic shift) 2D band relative to monolayer graphene [92]. The G band intensity increases almost linearly with an increase in the number of layers [93], while the 2D peak profoundly changes its shape, making it great for the identification of the number of layers up to five. The intensity of the D peak depends on the structural defects. If graphene or graphite is of good quality, no Raman D band is observed, which corresponds to the absence of the graphene structural defects (Fig. 5.4.6a). Thus, the most striking differences of the Raman features in monolayer graphene compared to graphite are as follows: (a) the 2D peak is single and sharp; (b) the FWHM of the 2D peak is ~30 cm^{-1}; (c) the ratio of the intensities of the 2D and

G peaks is ≥ 2; (d) the G peak position of graphene has a slightly lower wavenumber than for graphite (Fig. 5.4.6a) [3].

A comparison of the Raman spectra of graphene obtained by micromechanical exfoliation, rod rubbing, substrates rubbing, and CVD methods is shown in Figure 5.4.6b.

Besides, Raman spectroscopy also gives important information about doping, edge type, strain and stress, disorder, oxidation, hydrogenation, chemical functionalization, electrical mobility, thermal conductivity, electron–phonon and electron–electron interactions, magnetic field, and interlayer coupling [94]. For instance, the G peak is lowest when the Fermi level of graphene is at the Dirac point, and when the electron or hole concentration increases, the G peak has a blue shift. The G band width reaches a maximum when there is no doping in graphene and decreases for the increase of n- or p-doping in graphene [95].

Despite the fact that the Raman signal from graphene is strong and comparable to that of bulk graphite, investigating properties of graphene, graphene nanoribbons, or single carbon nanotubes at the nanoscale is not always easy due to the optical diffraction limit of laser beams. TERS is a rising star to investigate properties of materials at the nanoscale. For example, Gadelha and colleagues used TERS to identify local strain and doping in in-plane homojunctions in graphene devices, built as van der Waals heterostructures where half of the graphene sits on talc and the rest sits on SiO_2 [96]. The high spatial resolution of TERS enables the observation of the charge depletion region at the interface between different substrates [97]. Recent experiments show possible TERS resolutions of 1 nm or even below to (sub)molecule resolution [98].

Besides graphene, there are still a large number of semiconducting TMDCs, such as MoS_2, GaSe, InSe, $MoSe_2$, WS_2, WSe_2, etc. For MoS_2, the most-studied TMDC material, two main peaks, $E^1_{2g} \sim 382\,\mathrm{cm}^{-1}$ and $A_{1g} \sim 406\,\mathrm{cm}^{-1}$, are used to identify the number of layers. E^1_{2g} and A_{1g} correspond to in-plane and out-of-plane vibrations, respectively. With increasing flake thickness, the E^1_{2g} peak exhibits a red shift, but the A_{1g} peak shows a blue shift [27]. The blue shift in the A_{1g} peak can be explained by the van der Waals interaction between layers that suppresses the atom vibration, resulting in stiffening of the vibration. On the contrary, the E^1_{2g} peak's red shift suggests that the stacking-induced structure changes or long-range Coulombic interlayer interactions in multilayer MoS_2 affect the change of atomic vibration [99] stronger than the increase in van der Waals force [100]. Similar phenomena for E^1_{2g} and A_{1g} modes also have been observed for other 2D materials such as $MoSe_2$, WSe_2, WS_2. Even though E^1_{2g} and A_{1g} are good indicators for flake thickness, this method is limited to approximately four layers, and the shift is small and can also be affected by strain, doping, and substrate material. Another way is using the interlayer shearing and breathing modes, which are shown in Figure 5.4.7. These modes are sensitive to layer thickness, and most of the few-layer 2D materials are predicted to have these modes [101], so interlayer shearing and breathing modes can be used to identify the number of layers [16]. The disadvantage of this method is that the interlayer shearing and breathing

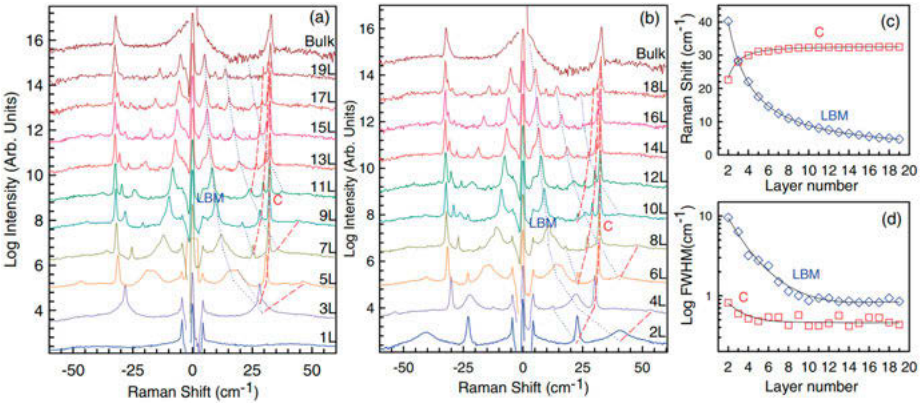

Figure 5.4.7: (a) Stokes and anti-Stokes Raman spectra of odd N layer (ONL)-MoS_2 in the low-frequency range. (b) Stokes and anti-Stokes Raman spectra of even N layer (ENL)-MoS_2. The spectrum of bulk MoS_2 is also included in (a) and (b). Dashed and dotted lines in (a) and (b) are guides to the eye. (c) Position of typical shear (C) and layer breathing (LB) modes as a function of *N*. (d) FWHM of C and LBM as a function of *N*. Solid lines in (c) and (d) are guides to the eye. Reprinted (adapted) with permission from Ref. [102].

modes appear at low Raman shifts, so it requires an additional triple stage spectrometer or a single-stage spectrometer with recently developed Bragg notch filters to record these modes [101]. For MoS_2, the number of layers can be determined by this method up to 14 layers.

The disorder in graphene can be quantified by the I_D/I_G peak intensity ratio in graphene spectra. Several groups have reported the effect of strain in 2D materials such as graphene, MoS_2, or GaSe. In the case of GaSe, the forbidden Raman mode located at 250 cm^{-1} is observed on the strained region created by a step on the HOPG substrate. This peak is not observed on plane and bulk GaSe [103]. Uniaxial strain is reported to cause red shift and splitting of the E^1_{2g} mode into two subbands E^{+1}_{2g} and E^{-1}_{2g} in MoS_2, WS_2, WSe_2, and $MoTe_2$ [104, 105]. The A_{1g} Raman mode of MoS_2 is sensitive to doping. The A_{1g} peak becomes weaker and broader with an increase of n- or p-doping concentration. In contrast, the E^1_{2g} peak is insensitive to doping, so the A_{1g} phonon vibration is typically used to investigate doping in MoS_2 [106]. In the case of WS_2, the out-of-plane A_{1g} mode of p-doped or n-doped WS_2 shows the red shift and blue shift, respectively, in comparison with undoped WS_2 [107, 108].

Photoluminescence

PL spectroscopy is one of the most widespread techniques in 2D material science along with Raman spectroscopy and the other advanced methods listed in this chapter. PL spectroscopy is based on a fluorescence effect, when an observed material illuminates

under irradiation. In general, PL spectroscopy allows to investigate electronic properties, a material's structure, and a presence of impurities with submicron spatial resolution.

For instance, [109] investigated the lifetime of PL and fluorescence on CVD-grown MoS_2. In the case of PL, the measurement was performed with a 532 nm continuous laser on a $75 \times 75\,\mu m^2$ range with 375×375 points that results in a high-quality image, shown in Figure 5.4.8. In Figure 5.4.8a the authors demonstrate a PL map of the region of interest where MoS_2 flakes are grown. Dark regions here are the results of nonphotoactive areas, which are cracks or grain boundaries. Figure 5.4.8b shows a PL map of MoS_2 flakes that do not reveal grain boundaries or stress-related cracks. Hence, PL mapping is a useful method for investigating the material's defects.

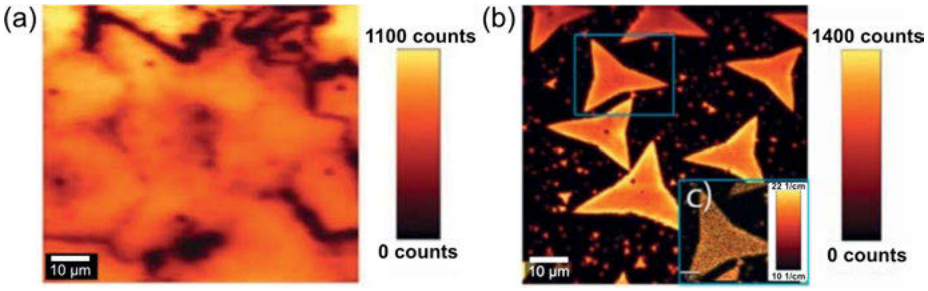

Figure 5.4.8: (a) Total PL map and (b) PL map of clearly seen MoS_2 flakes on the substrate. Reprinted (adapted) with permission from Ref. [109].

Another clear experiment aimed at revealing defects was made by Xu et al. [110]. They studied the PL behavior of high-quality MoS_2 single layers. In this work, a MoS_2 monolayer was measured by PL spectroscopy under different temperature and air/vacuum conditions. Figure 5.4.9a demonstrates a common PL map of a flake on a sapphire substrate. Obviously, the PL map contains several regions with lower PL intensity along the crystal edges. The authors suggest that these fluctuations in PL intensity may be related to the varying material quantity at the edges or contaminants from air (such as dust). But, in general, the PL image shows the material with a homogeneous structure, which is also proven by Raman imaging on this flake in the inset. The authors also discussed a relationship between PL intensity and ambient conditions, such as the presence of air. Decreasing PL intensity is connected with interaction of oxygen or nitrogen from air and sulfur vacancies in MoS_2 and leads to recombination of photogenerated charge carriers. Particularly, the lowering of PL intensity with increasing temperature signals a higher number of nonradiative recombinations. In addition, the peak positions of the PL express a hypsochromic shift while temperature decreases, depicted in Figure 5.4.9c. This blue shift is related to the widening of the band-gap, caused by lattice shrinkage and lower thermal relaxation ability.

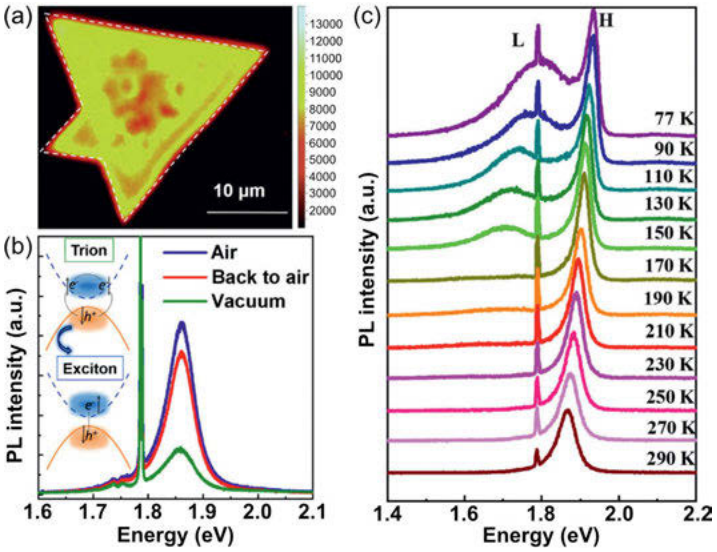

Figure 5.4.9: (a) PL map of high-quality MoS_2. (b) PL spectra of the flake being exposed by air/vacuum. (c) PL spectra of MoS_2 flake under various temperature. Reprinted (adapted) with permission from Ref. [110].

TERS

One powerful method for the investigation of 2D materials properties is TERS. In TERS, the Raman spectrum is amplified when a gold- or silver-coated tip approaches the illuminated sample surface. Using the AFM cantilever as an amplifier, the physical and chemical properties of the 2D materials could be measured in the nanorange with an integrated Raman spectrometer while obtaining topographic data by a coupled AFM system.

In 2013, Su et al. [111] performed a TERS investigation of SLG flake edges obtained by the Scotch tape method from HOPG. The far- and near-field spectra shown in Figure 5.4.10a were recorded in the middle of the SLG to avoid artifacts caused by intensity changes near the edge. The disappearance of peak D in Figure 5.4.10a indicates the absence of defects in the measured spots. Figure 5.4.10b shows an AFM lateral force image acquired simultaneously with a TERS image. Mechanically exfoliated graphene flakes have been found to have sharp and linear as well as jagged and indeterminate edges. A 2D TERS image of the same area is shown in Figure 5.4.10c.

The authors discovered that the graphene D peak intensity (Fig. 5.4.10d) could be used to accurately determine the SLG edge location, and the phase-breaking length (path length of conduction electrons while maintaining phase coherence) can be precisely measured by using TERS. The phase-breaking length was measured to be

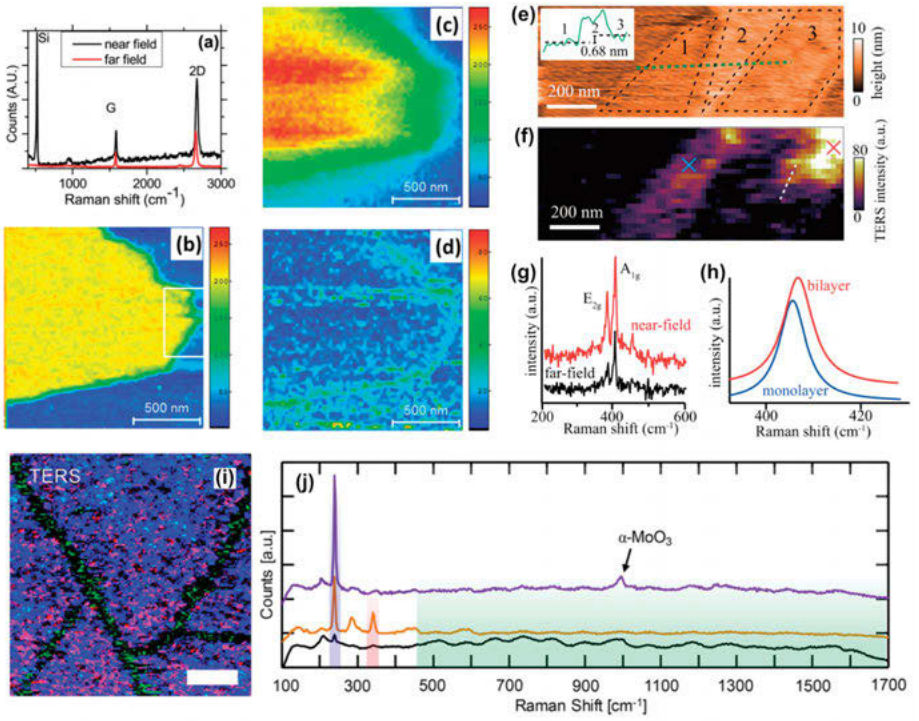

Figure 5.4.10: (a) Tip-enhanced and confocal Raman spectra of a monolayer graphene flake. (b) AFM lateral force image of monolayer graphene recorded during TERS mapping. (c) TERS image formed using the 2D peak height. (d) TERS image formed using the D peak height. Image size: 1.5 µm × 1.5 µm, 60 × 60 pixels. Reprinted (adapted) with permission from Ref. [111]. (e) AFM image of the region of interest. Topographic line profile along the green dotted line is shown in the inset. (f) TERS intensity map of the A_{1g} mode for the same area as that in (e). (g) Near-field and far-field Raman spectra of the MoS_2 layer taken at the same position. (h) Lorentzian fitted TERS spectra of the A_{1g} mode. Reprinted (adapted) with permission from Ref. [112]. (i) Combined TERS maps of $MoSe_2$ polycrystalline monolayer. (j) Averaged TERS spectra showing resonant response (orange), nonresonant response (purple), and signal from the grain boundaries regions (black, showing significantly decreased intensity of Raman signal of $MoSe_2$ over the grain boundaries). Reprinted (adapted) with permission from Ref. [113].

4.2 nm, which is much smaller in comparison with far-field Raman results with a value of 30–50 nm.

Kato et al. [112] investigated atomically thin MoS_2 layers on a glass substrate by TERS coupled with AFM. It was revealed that the inhomogeneous features of the thin MoS_2 layers originate from mechanical and chemical preparation methods.

Figure 5.4.10 demonstrates AFM (e) and corresponding TERS (f) images as well as Raman (g) and Lorentz-fitted spectra constructed using the intensity of the A_{1g} mode (h). In this work, TERS intensity denotes the near-field Raman intensity, which is obtained after subtracting the far-field intensity. Spectral changes of the near-field Ra-

man signal locate the presence of nanometer defects and residual substances with a high spatial resolution of ~20 nm, which would not be visible without TERS using only far-field Raman spectroscopy, since its nanometric volume is much smaller than the diffraction-limited focus spot.

Another interesting work is related to TERS measurements of poly- and monocrystalline $MoSe_2$ monolayer films synthesized by CVD and transferred to gold substrates [113]. Here the authors claim that based on TERS results the concentration of the charge carriers in the grain boundaries of $MoSe_2$ flakes is increased in comparison with the interior of the as-grown monolayer crystals. Also, a decreased capacitance and TERS signal are observed at these boundaries after transferring to the gold substrates.

High-resolution resonance TERS measurements of $MoSe_2$ are performed as shown in Figure 5.4.10i and j. The appearance of the peak at 995 cm^{-1} is attributed to the presence of α-MoO_3. The authors conclude that nanoscale inclusions of MoO_3 in the $MoSe_2$ matrix are responsible for the abovementioned observations. The high spatial resolution of TERS allowed to see differences in nanoscale domains in layered $MoSe_2$ and to reveal significant inhomogeneity where uniform spectral distribution is observed by confocal Raman microscopy.

5.4.4.4 2D hybrid atomic heterostructures and devices

This section focuses on 2D hybrid atomic heterostructures and devices consisting of various 2D atomic layers, their synthesis, and their nanoengineered properties.

After the isolation of 2D atomic materials it became possible to form 2D hybrid heterostructures based on these for application in 2D devices. As semiconductor heterostructures have a great influence on our daily life, the Nobel Prize in physics was awarded to Zhores Alferov and Herbert Kroemer in 2000 for the discovery of semiconductor heterostructures [2, 115]. Traditional heterostructures usually consist of semiconductors only, while 2D hybrid heterostructures include different 2D atomic layers, such as metallic graphene, insulating h-BN, and semiconducting TMDCs. As an atomic layer can be considered to consist of the surface only, the single atomic layers in the hybrid heterostructure behave as independent entities. The simplest 2D heterostructure consists of double atomic layers [116] such as stacked graphene and h-BN (graphene/h-BN), MoS_2/graphene, and WSe_2/h-BN, while a trilayer heterostructure consists of triple atomic layers such as stacked semiconductor TMDC, dielectric h-BN, metallic graphene (MoS_2/h-BN/graphene), WSe_2/$MoSe_2$/graphene, etc.

Due to a large number of 2D materials, different atomic heterostructures with electronic properties ranging from insulators, semiconductors, and metals to superconductors can be prepared, enabling a greater number of combinations than traditional heterostructures. As nanolayers are self-passivated [117], i. e., their surfaces are free of chemically active dangling bonds, the formation of hybrid 2D heterostructures with

high-quality heterointerfaces is possible. Atomic layers in the heterostructures interact via weak van der Waals forces, which allow for stacking dissimilar layers with very different lattice constants. For example, even though the large lattice mismatch between graphene and WSe_2 is 23 %, the formed WSe_2/graphene nanoheterostructure shows an atomically sharp interface and nearly perfect crystallographic orientation. The complexity of the 2D heterostructures can be tailored, and different heterostructure devices with desired band alignment can be fabricated [114].

2D layers can reassemble into multilayers or monolayer stacks and form vertically or horizontally stacked heterostructures. Vertically layer-by-layer stacked monolayers are called vertical 2D heterostructures, and monolayers stitched together in a plane are called lateral 2D heterostructures. These 2D heterostructures are also called van der Waals heterostructures as the van der Waals interaction serves as a "weak glue" in the stack.

The vertical 2D heterostructures have different atomic layers that are vertically stacked with various architectures and functionalities such as stacks of graphene (G) on h-BN (G/h-BN) [118], h-BN on graphene (h-BN/G), graphene on TMDC (G/TMDC), TMDC on TMDC (TMDC/TMDC), etc. The lateral 2D heterostructure is an atomically thin structure which consists of different 2D atomic layers arranged in one plane and allows the formation of clean interfaces. For example, monolayers of graphene and h-BN can be assembled and form lateral G/h-BN heterostructures with clean interfaces due to the same crystal structure. The major appeal of the lateral heterostructures for electronic applications certainly lies in their atomically thin nature that offers a wider world of new nanomaterials with various functionalities and opens up new opportunities for 2D atomic devices [119]. They have been demonstrated for use in flexible, transparent, low-power electronics and optoelectronics, such as lateral atomic p-n diodes [120], lateral Schottky diodes [121], lateral p–n junction photodetectors [122], and lateral heterostructure FETs [123], as well as providing a high potential for future high-density atomically thin integrated circuits [124]. 2D hybrid atomic heterostructures with different architectures, such as stacks of various 2D atomic layers with different order and composition, can be formed by both mechanical stacking and direct epitaxial growth methods which are considered below.

The mechanical stacking method allows forming stacks of 2D atomic layers and their hybrid heterostructures. For that purpose, the mechanically or chemically exfoliated atomic layers are mechanically transferred and after manipulation layer-by-layer stacked on the appropriate substrate. During manipulation of the atomic layers the transferred second atomic layer is precisely stacked (aligned) on the first one by a micromanipulator under an optical microscope. As a result, two different atomic layers are attached closely by van der Waals forces. After further continuation of the transfer-stacking process a stack, and finally a multilayer 2D hybrid heterostructure, is formed.

The direct epitaxial growth of 2D hybrid heterostructures is an alternative to the mechanical stacking method. The CVD method (see Section "Synthesis of 2D atomic materials" above) allows direct epitaxial growth of various vertically (out-of-plane)

and laterally (in-plane) stacked 2D hybrid heterostructures [125]. CVD-grown 2D stacks can be formed in two ways: (a) sequential multistep epitaxial growth of atomic layers on the substrate and (b) growth of atomic layers separately on the substrate, followed by layer-by-layer transfer and stacking. Vapor-phase growth of 2D heterostructures has much in common with 2D atomic materials growth and is an effective way to obtain 2D materials. Compared to the growth of graphene and h-BN, the vapor-phase growth of TMDCs is less controlled and has poor repeatability. Van der Waals epitaxy refers to the epitaxial growth of layered materials on clean surfaces without dangling bonds, even if there is a large lattice mismatch between the two atomic layers [83]. Now we are in the initial stages of forming and characterizing van der Waals heterostructures. CVD, direct growth, and van der Waals epitaxy methods have already been used for growing different atomic heterostructures [126].

During the fabrication of 2D hybrid heterostructures by mechanical stacking and CVD methods, the layer-by-layer mechanical transfer and stacking causes cracks and contamination to the 2D layers and their interfaces. Nowadays the existing wet [69] and dry [70] transfer methods for forming 2D layers (e. g., graphene, MoS_2) and heterostructures (e. g., graphene/MoS_2 stacks) can lead to uncontrollable atomic layer and heterointerface contamination as adsorbates. Hydrocarbons get absorbed or trapped between the atomic layers. Thus, they may not result in high-quality 2D layers with clean interfaces and 2D hybrid heterostructures with improved characteristics. Therefore, the development of alternative and nonconventional methods for obtaining 2D hybrid heterostructures is important.

The rod [75, 76] and substrate [48, 71, 72] rubbing methods, which are discussed in the Section "Synthesis of 2D atomic materials," may offer an alternative to the transfer-stacking and CVD growth methods. Mechanical methods allow for obtaining lateral and vertical 2D hybrid heterostructures with clean and sharp interfaces on many substrates, with no need for transfer after the formation [49, 127].

Herbert Kroemer, the Nobel Prize winner in Physics in 2000, stated that "the interface is a device" [128]. More than a decade later, Andre Geim and Irina Grigorieva experimentally confirmed that statement, which has opened up new opportunities at the interface of bulk materials. As a result, 2D heterostructures with the desired energy band alignment can be designed by combining various metallic, semiconducting, or insulating 2D atomic layers in the lateral or vertical geometries. This allows forming different atomic heterojunctions with novel functionalities at the nanoscale. The interface of the heterojunction between two atomic layers can be tuned by selecting the 2D materials, applying electric fields, elastic strain, etc. Moreover, the physical properties of atomic heterostructures can be tailored at the nanoscale by the heterogeneous nanoengineering of the interlayer stacking distance, order and orientation, material and number of constituent atomic layers, band structure of the junction interfaces, etc. For example, changing from AA (AA-stacking implies that corresponding atoms in different layers have the same lateral coordinates) to random stacking, the band

structure changes from direct to indirect [129]. As a result, heterostructures with clean atomically sharp interfaces will have unprecedented tunability.

The reproducible formation of high-quality heterointerfaces between 2D layers and the control over their location, number, orientation, and stacking order of atomic layers still remains challenging. Even a single atom out of place can strongly affect the properties of the atomic layers. Thus, the quality of the heterolayers and heterointerfaces can be controlled by tailoring the disorder structure at the atomic scale, such as substitutional defects, grain boundaries, anisotropy, or stacking misalignment.

2D materials have tunable band-gaps, which are strongly dependent on the number of the atomic layers in the stack, and can be altered to produce a range of gap energies. The change in the band structure with the change of the number of atomic layers is due to quantum confinement and the resulting change in the hybridization [130]. Novel tunable heterostructure devices can be fabricated by nanoengineering their band-gap. This way, new exciting opportunities and advantages (extremely high surface area, flexibility, etc.) open up for designing and fabricating next-generation devices with improved characteristics. Recently, Xue et al. demonstrated large-scale production of a vertical MoS_2/WS_2 heterojunction in multiple layers by two-step sulfurization of patterned WO_3 and Mo sheets using a thermal pressure reduction process. Based on the grown heterojunctions, arrays of photodetectors were fabricated and a photoresponse was realized on both rigid and flexible substrates [131]. In another work by Xu et al., the authors show the development of a hybrid 2D graphene-MoS_2 phototransistor with high responsiveness due to the combination of the advantages of strong MoS_2 light absorption and high mobility of graphene carriers. The main mechanism is explained by the photoexcited hole transfer from MoS_2 to the graphene layer when exposed to light. The photoexcited holes generated from the MoS_2 flakes are transported into the graphene under the action of the increasing electric field; meanwhile, the electrons are trapped in the MoS_2 flakes, creating an additional p-type photoexcitation effect for the graphene located below them [132]. Xiong and coauthors demonstrated a multifunctional nonvolatile logic-in-memory application based on novel 2D heterostructures: black phosphorus/rhenium disulfide (BP/ReS_2) [133]. The van der Waals heterostructure and device characterization are presented in Figure 5.4.11. The synaptic weight change is one of the characteristics of artificial synaptic devices, which are memristor-based devices mimicking biological synapses, and they are used in neuromorphic computing systems that process information in a parallel, energy-efficient way and store information in an analog, nonvolatile form. A record-high synaptic weight change, i. e., a change in the strength in the connection between two nodes, over 10^4 % has been shown in the devices. Neural network simulations for handwritten digits recognition based on the heterostructure devices were successfully implemented with a recognition accuracy of around 90 %.

The spectroscopic analysis of heterostructure features such as strain and defect concentration is analogous to that of monomaterial layers. However, the number of

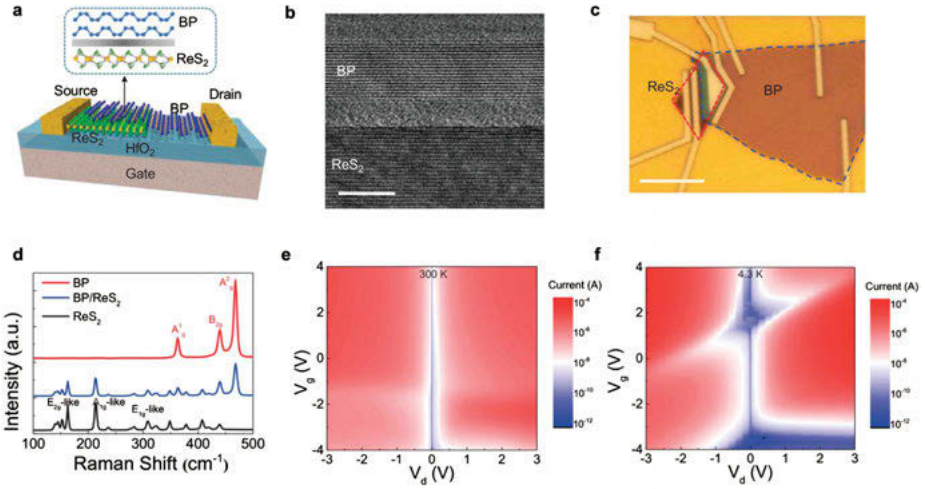

Figure 5.4.11: Van der Waals heterostructure and device characterization. (a) Schematic illustration of a BP/ReS_2 heterostructure device and schematic lattice cross-section of the junction interface. The drain electrode is deposited on the BP layer and the source on the ReS_2 layer. (b) Cross-section HR-TEM image of the BP/ReS_2 interface. A PO_x layer of about 4 nm thick can be observed. The scale bar is 10 nm. (c) Device morphology in an optical microscope. Scale bar: 10 μm. (d) Raman spectra of BP, overlapping BP/ReS_2, and ReS_2 regions, respectively. Current of the BP/ReS_2 junction with different V_d and V_g bias at (e) 300 K and (f) 4.3 K. Reprinted (adapted) with permission from Ref. [133].

layers may prove harder to be identified: the spectroscopic methods may need to be recalibrated due to electronic structure changes in heterostructures that define the Raman and PL sensitivity to the number of layers.

5.4.4.5 Applications of 2D atomic materials and devices

Thanks to their unique properties, 2D atomic materials have the potential to revolutionize many technologies, in areas such as materials and composites, energy, health, space travel, etc., in the same way that graphene promises to do. The various applications of 2D materials mentioned throughout the chapter so far mostly appear as proofs-of-principle in research papers and include (a) wearables (flexible electronics, smart textiles, etc.), (b) mobile and data communications (computer circuits, data storage, ultrafast transistors, optical modulators, etc.), (c) displays (touch screens, conductive inks, transparent electrodes, coatings, light sources, etc.), (d) energy (solar cells, advanced batteries, supercapacitors, fuel cells, hydrogen cells, etc.), (e) transport (corrosion-protective coatings, ultrastrong composites, etc.), (f) environment (desalination membranes, monitors, biofuel, etc.), and (g) food and health (water filters, biosensors, drug delivery nanocarriers, food safety monitors, DNA sequencers, etc.). Still, graphene is the one that currently does have

commercial applications, where however in many cases graphene flakes are merely admixed into other materials, e. g., (a) wearables (graphene-enhanced mechanical watches [Richard Mille, France], bracelets with curved graphene film touch sensor [Wuxi Graphene Films, China], graphene-enhanced shoes [inov-8, UK], cycling shoes [Catlike, Spain], graphene-enhanced sportswear with graphene-assisted heat management [Directa Plus, UK, Colmar, Italy], graphene-based smart textiles [Versarien plc, UK, GrapheneUP, Czech Republic, Grafren AB, Sweden], graphene-based fabrics, wearable sensors [GrapheneUP, Czech Republic], graphene-enhanced clothing [Graphene-X, Hong Kong], graphene-coated bulletproof jackets [Vollebak, UK]), (b) mobile and data communications (graphene-based smartphones with flexible touch screen [Galapad Settler, Chongqing Graphene Technology Company, China], bendable graphene smartphones [Moxi Group, China], smartphones with graphene film as a heat sink for cooling [Huawei], graphene integrated circuits [IBM], graphene-based flash memory [University of California, USA]), (c) displays (graphene screens with touch screen panel [Huayuan Display, China; Wuxi Graphene Films, China; Chongqing Graphene Technology, China], updatable foldable electronic newspapers based on graphene-based electronic paper [e-paper] with graphene-based flexible displays [Guangzhou OED Technologies, China], the largest newspaper-size flexible e-paper [LG Display, Korea], e-paper-based touch screens [Sony], graphene e-paper displays [Plastic Logic, Germany]), which have potential for application in next-generation e-readers/books, cell phones, music player displays, smart card displays, wearables (clothing, watches, military), consumer electronics, etc., (d) energy storage (graphene solar cells [IDTechEx, UK], graphene-enhanced lithium [Nanotech Energy, USA] and aluminum-ion batteries [Graphene Manufacturing Group, Australia], graphene anodes and cathodes for lithium-ion batteries [Nanotech Energy, USA], graphene supercapacitors [First Graphene Limited, Australia], graphene power banks [Real Graphene, USA]), (e) transport (graphene-coated airplanes and airplane wings [Haydale Composite Solutions, UK], graphene-coated cars [Briggs Automotive, UK], graphene car wheel arches [Torque, Singapore] and wheels [Vittoria, Italy], anticorrosion and antierosion graphene-enhanced coated cargo ships [Talga Technologies Ltd., Australia], 3D-printed graphene-infused arch structures over railways [AECOM, USA], graphene-enhanced coated satellites with regulated temperature [from too hot to cold] [SmartIR Ltd., UK], graphene-based rockets [Orbex, UK]), (f) environment (graphene membranes [Perforene, Maryland], graphene-ceramic coatings for cars [Adam's Polishes, USA], graphene-based anticorrosive and moisture penetration blocking paint and coatings [Applied Graphene Materials, UK], graphene-enhanced rubber, ink, and coatings [Vorbeck Materials Corporation, USA]), (g) food and health (graphene biosensors [Cardea, USA], functionalized graphene ink for biomedical sensors [Haydale, UK], graphene face masks [Medicevo Corporation, USA]), (h) electronic components and devices (graphene-enhanced earphones [ZOLO, India], headphones [Ora Graphene Audio, Canada], and earbuds [MediaDevil, UK],

solid-state drives with graphene heat spreaders [TeamGroup, Taiwan], graphene-enhanced curved light bulbs and lamps [Graphene Lighting, UK], graphene FETs [BGT Materials, UK], graphene FET arrays [Graphenea, Spain], all-graphene optical communication links [modulator and detector] [Graphene Flagship], graphene-based photodetectors [Emberion, Finland], graphene sensors [Biolin Sientific, China]), and (i) different products (cement [Versarien, UK], tennis racquets and skis [HEAD, Austria], bicycles [Dassi, France], helmets [Momodesign, Italy], tires [Vittoria, Italy], graphene-enhanced fishing rods [G-Rods, USA], graphene bows [Win & Win Company, Korea], etc.).

At the beginning let us consider graphene layers as a coating and membrane. Graphene is composed of sp^2 hybridized carbon atoms with high electron density in the aromatic rings. The internuclear pore size considering the van der Waals radius of carbon is 0.064 nm [134]. The latter is smaller than the van der Waals radius of small atoms and molecules like helium (0.14 nm) and hydrogen (0.157 nm). As a result, pristine graphene can be considered as the thinnest coating or ultimate impermeable membrane for gases and liquids, which due to its high mechanical strength can withstand even when a 1 to 5 atm pressure difference is imposed across its atomic thickness at room temperature [5]. An impermeable membrane can become permeable after modifying it, i. e., opening artificial nanopores in it by top-down (e. g., hole drilling by high temperature oxidation, electron beam, UV irradiation, plasma bombardment) or bottom-up (e. g., self-assembly) methods [135]. The main function of a permeable membrane is to effectively separate molecules and ions from a mixture. The membranes can have two main structures: monolayer and stacked multilayer. Graphene membranes can be used for dialysis, filtration, and separation of gases and solvents [133], such as separating organic solvents from water, removing water from gas, removing carbon dioxide in the atmosphere, etc.

By combining flexibility and stretchability with its impermeability to all gases and liquids a graphene layer can be considered as a barrier layer or coating. Some of the existing hazardous anticorrosion materials (hexavalent chromium, cobalt, cadmium, etc.) of metal coatings have recently been fully restricted because of their carcinogenic risk and biocidal properties or classified as toxic [27]. When replacing them with chemically passive graphene layers, the latter can serve as a protective coating due to its good chemical resistance, impermeability to gases, adsorption capacity, antibacterial properties, mechanical strength, lubricity, and thermal stability [27]. MFL graphene acts as a protective coating against (a) water and oxygen, reactive gases, liquids, salts, acids, and microbes or (b) adsorption of toxicants, chemical contaminants, and hazardous gases (i. e., CO, NH_3) from the environment. For example, graphene coatings can stop the transfer of water and oxygen, thus keeping food, perishable goods, or pharmaceutical packaging fresh for longer. The methods for preparation of graphene protective coatings include CVD, high-temperature pyrolysis of organic molecules, rapid thermal annealing, electrophoretic deposition, powder spray (electrostatic powder coating, plasma spray coating), solution spray, dip coating, spin coat-

ing, drop casting, vacuum filtration, and brushing [27]. However, there is no unique coating technique that is effective for all applications [27]. For example, CVD-grown graphene is not suitable for corrosion resistance applications for long periods due to a high numbers of grain boundaries, folds, wrinkles, and point defects on the coated surface [27].

The most widespread graphene applications employ composites. Composite materials are formed by combining two or more materials with different properties to make a resulting material with unique characteristics. To obtain graphene-based nanocomposites (mixture of graphene with other materials, including metal nanoparticles, polymers, plastics, small molecules, etc.) graphene should be incorporated and then homogeneously distributed into them [83]. The resulting composite typically shows higher mechanical strength. Additionally, graphene–polymer composites are flexible and good electrical conductors, while ceramic–graphene composites, i. e., SiC-, Si_3N_4-, Al_2O_3-, BN-graphene, etc., enhance electrical properties, thermal conductivity, and refractory, mechanical, antifriction, anticorrosive, and biocompatible properties. Graphene-based composites can be applied in satellites, in the sun's environment as probes, in Li-ion batteries, sensors, supercapacitors, fuel cells, and solar cells, for photocatalysis and corrosion protection, in medical implants, in aerospace materials, etc. However, only some of the mentioned applications have started to see commercial realization, such as electrode materials for Li-ion batteries (anodes and cathodes) [136].

Some further graphene-based electronic devices, such as batteries, supercapacitors, solar cells, touch screen displays, bendable smartphones, sensors, light-emitting diodes (LEDs), and transistors are just beginning to appear. Let us consider a few of them.

The 2D nature of graphene becomes relevant for the enhancement of charge storage by using graphene batteries and supercapacitors, and for energy generation by using graphene-based solar cells, which will be discussed below. Batteries have long been the Achilles heel in energy storage as they are heavy, have long charging times (minutes), and lose charge capacity over time. As graphene is the thinnest material with the highest surface area-to-volume ratio, it potentially can store tremendous amounts of energy, reduce battery charging times (to seconds), prolong lifetime, and lower weight and waste. The first graphene-based batteries were demonstrated in 2014 [37, 137]. Next-generation batteries will move away from electrochemical cells (for example, lithium-ion) towards supercapacitors. A supercapacitor or electric double-layer capacitor stores energy in an electric field instead of in a controlled chemical reaction like batteries. Graphene supercapacitors are flexible, light, durable, consistent across a wider temperature range, and environmentally friendly (without using lithium). They provide high power, while using much less energy than conventional devices. As graphene supercapacitors are light, they can be charged in seconds and store more energy in a smaller space, and they can reduce the weight of smart phones, cars, airplanes, etc. Nowadays graphene supercapacitors are much more expensive

than graphene batteries, and by decreasing their cost the batteries could be replaced by supercapacitors, revolutionizing this field.

The integration of 2D materials into optoelectronic devices, such as solar cells, is promising for energy generation, as they are hundreds of thousands of times thinner and lighter than silicon ones and absorb a significant amount of photons per atomic layer. For example, monolayer graphene has a broadband light absorption of 2.3 % below the energy of 3 eV that linearly scales with the number of atomic layers [60]. The main challenge for the durability of the standard solar cells is the exposure to different weather conditions due to which they become less efficient with time (though their lifetime is ~40 years) and as a result they have to be replaced. The combined properties of graphene and other materials could improve the efficiency of solar cells and favor the fabrication of flexible and rollable solar cells. The latter can be wrapped to fit any product, such as building roofs, automobile bodies, furniture, clothing, etc. Due to its transparency, mono- and bilayer graphene can be used as both an optically active medium and transparent conductive electrode or coating material in graphene-based solar cells. Graphene also can improve the performance of perovskite solar cells, the stability of which is still low due to their degradation in air and humidity upon continued exposure to sunlight and heat [138].

Many electronic devices rely on costly platinum- or indium tin oxide (ITO)-based conventional electrodes, while most portable devices with touch screen displays rely on ITO coatings. Although both ITO electrodes and coatings are popular, they have various drawbacks: they are brittle, not fully transparent (85 % of visible light, compared to 97.7 % for graphene), chemically unstable, and costly, they have a high refractive index, and indium has a limited availability. For example, nowadays plasma TVs and portable devices, such as smartphones and tablets, have thick, inflexible (ITO is layered on glass to protect them), and expensive (the most expensive component of the portable devices) ITO displays or screens. Furthermore, since graphene is mechanically strong, transparent, ultrathin, highly conductive, and flexible, it can be an alternative to conventional ITO electrodes and coatings.

Another futuristic application is smart windows. For example, at the flick of a switch (a) smart glass windows of buildings could block part or all sunlight, only heat, or both, helping control the temperature of buildings, (b) smart glass windows of cars could temporarily turn into a transparent display (for example, a car windscreen can light up to show you an urgent message), (c) transparent transistors on top of a contact lens could continuously monitor eye function (i. e., ocular pressure), etc.

2D materials are very sensitive to the environment and are ideal materials for sensors due to a large surface area-to-volume ratio and unique optical properties. Ultrasensitive 2D material sensors could detect dangerous compounds helping to protect the environment, reduce food wastage, prevent illnesses, protect crops, react to chemical warfare agents and explosives, etc.

Due to their outstanding properties, graphene and 2D materials are promising for biomedical applications, such as targeted drug and gene delivery, improved can-

cer treatment, biosensing, bioimaging, tissue or cell engineering, DNA sequencing, and "smart" implants. Currently the challenges are biodistribution, biocompatibility, and toxicity of 2D materials, which are either poorly studied or need to be tackled by functionalization. As functionalization improves the selectivity of graphene, graphene sensors can be used for biosensing, e. g., to detect biomolecules including glucose, cholesterol, hemoglobin, and DNA. They may be employed in food analysis, water testing, drug development, forensic analysis, medical diagnosis, environmental field monitoring, industrial process control, manufacturing of pharmaceuticals, etc. [139]. Bodily worn biosensors can collect data about the physical and chemical properties of the body and monitor day-to-day activity. Heat, humidity, salt, or pressure biosensors can be used in bed sheets to monitor a patient. Wearables act as extra accessories to the clothing and can be worn on the wrists, faces, ears, and feet. Wearables include smart glasses, smart watches, wristbands, lenses, smart fabrics, etc. For example, a graphene-based smart and wearable thermometer can continuously monitor the body temperature and be read out by a smartphone. Combined from the words "biology" and "electronic," bionic devices refer to devices that improve an organ or tissue, replacing organs or other body parts by mechanical ones. Bionic implants differ from simple prostheses by mimicking the original function very closely, or even surpassing it [140]. Bionic devices can be incorporated in living tissues or connected directly to neurons. Recent research demonstrates that CVD graphene material causes less inflammation, determined by the number of microglial tags, compared to biocompatible polymers. Therefore, graphene could be used in electrodes for retinal prostheses or even in any electronic devices for the registration and stimulation of the central nervous system. Graphene-based retina implants could allow blind people to see in the near future [141]. Graphene surfaces are more biocompatible compared to some traditional materials due to their flexibility and chemical durability, while toxicity mechanisms need further investigation since they strongly depend on the sheet size and functionalization. Thus, graphene-based medical devices may improve healthcare.

Silicon transistors have consistently become smaller and more powerful over the last few decades, following Moore's law. Subsequent reductions in the transistor scale will soon approach limits due to statistical and quantum effects and difficulty with heat dissipation [17]. Due to its outstanding properties graphene can be applied as an alternative to silicon. Graphene may allow microprocessors to produce very little heat and run at speeds several times faster than existing microprocessors [142]. Flexible ultrathin and ultrafast computers are still waiting to emerge. While graphene shows promise for transistors, due to the absence of a band-gap, graphene has a major drawback: it cannot switch the flow of electricity "off" like silicon. This means the current in graphene will flow constantly and it cannot serve as a transistor on its own. This main problem must be resolved before graphene can be employed as a transistor. There exist multiple approaches for opening and engineering the band-gap in graphene such as nanostructuring (formation of graphene nanoribbons, quantum dots, etc.), chemical doping and functionalization, applying a high electric field, changing the number

of the atomic layers, and introducing buffer atomic layers between two atomic layers. However, these modifications in graphene structures (a) cause a change in the electronic structure and result in the degradation of the electron transport properties of graphene and (b) add complexity and diminish the high mobility of graphene. For example, after functionalization of graphene, the sp^2 structure can be converted to sp^3 by converting metallic graphene to an insulator. Anyway, after these modifications the graphene transistor can be switched "on" and "off," but the speed of the electrons is slowed down somewhat. Semiconducting 2D materials are particularly useful here. The first graphene [143] and MoS_2 [144] FETs, as well as graphene integrated circuits [145] with graphene FETs were demonstrated. Due to downscaling of the length of the device or conducting channel in graphene or MoS_2 FETs short-channel effects become significant [146], which is an important challenge for the electronic industry. With the extremely small size of such structures, nanospectroscopic measurements allow to study the channel length scaling, clarify whether the reduced thickness is beneficial or detrimental to the contacts, and finally offer new insights and solve nowadays existing major problems, such as self-heating, hot carrier effects, interfacial effects between 2D layers, and usage of various architectures and geometries of the channel, which affect the electrical performance of the FETs. Combinations of graphene (as a channel material) and TMDCs (as photosensitive material) allow the fabrication of phototransistors. Recently only one atom thick and 10 atoms wide graphene transistors have already been created. The smaller the transistor size, the better they perform within circuits [147]. Still, graphene technology is a long way from the reliability and reproducibility of the established silicon-based technology, and will require significant development.

5.4.5 Some challenges and solutions

New advancements in the synthesis and characterization of 2D atomic materials and heterostructures, as well as their application in next-generation advanced technologies, are intensely pursued. Future flexible electronics technology will evolve from rigid devices to bendable, rollable, and foldable ones [31]. These devices are expected to be advantageous compared to rigid ones due to their better durability, lighter weight, lower material requirements, and improved comfort [31]. Multiple nanofabrication possibilities allow producing a great variety of new generation 2D hybrid multilayer heterostructures and flexible devices [48]. Nevertheless, until now we have seen only few commercial devices based on 2D materials, mostly with graphene. The reason for this is that there are still a lot of technological challenges toward 2D material devices and applications. Each specific application has its own requirements from synthesis to final products, for instance, electronics, photonics, optoelectron-

ics, twistronics, or solar cells require 2D material thin films with high crystal quality: thickness, defect concentration, grain size, etc.

Synthesis of 2D materials is the first critical step to build devices based on 2D materials. Despite many achievements in this area, there are still a lot of questions about scalability, quality, controlling the defects, and fundamental understanding of synthetic processes. Thickness control is critical for high-performance electronics. Nowadays, CVD, liquid exfoliation, and wet chemical synthesis are the most popular methods to synthesize 2D materials on a larger scale. Wafer-scale polycrystalline monolayer and multilayer graphene films have been successfully synthesized. Still, some major challenges in 2D material device fabrication remain: growing 2D materials (in large volumes or over large areas with a consistent quality), making Ohmic contacts (to minimize parasitic effects) and passivation layers, controlling the etching (to achieve sophisticated device structures), and improving the quality of the atomic layers and heterointerfaces of the heterostructure devices. Besides, now most research is focused on inorganic 2D materials (with graphene as a pure allotrope of carbon being considered as inorganic, too), while later on organic ones also should be considered. In order to achieve such results, it is also necessary to evolve existing spectroscopic methods and develop new ones for a more detailed investigation and characterization of 2D materials on the basis of which new devices will be built. These methods are capable of delivering information not only about the defects, electron–phonon coupling, number of layers, and contamination, but also about lattice orientation and edge types. Most significantly, nanoscale methods such as TERS and nano-IR can provide this information at the scale of the device channel and grain edges. Opportunities are plenty, but there will be many challenges ahead, in particular since some of the details of these methods are still poorly understood. Investigating the fundamentals of spectroscopic methods in application to 2D materials and improving spatial, temporal, and spectral resolution and sensitivity will be necessary as well as engineering new nanosystems for gaining basic knowledge of light–matter interaction and energy flow at the nanoscale. These small sample volumes also require extreme sensitivity. Finally, these approaches are experimentally complex, and the methods need to be developed further to make them user-friendly. 2D materials in particular are ideal targets for fundamental TERS studies since TERS overcomes two main drawbacks for conventional Raman spectroscopy, which are a low signal response and a limited spatial resolution. This in turn allows us to obtain much more detailed results for the investigation and characterization of 2D material properties.

5.4.6 Summary and impact

The twentieth century was the age of plastics, while the twenty-first century may become the age of graphene [11]. Maybe one day we will talk about “graphenes” as we

now speak of "plastics." In the twentieth century, our life completely changed by replacing older materials, such as metal and wood, with plastics. New possibilities might lie ahead if graphene and other 2D materials lead us to ultralight, ultrathin, strong, optically transparent, electrically conducting, and semiconducting materials. To date, they show great promise due to the variety of properties and high-quality interface formation. Graphene and 2D materials may likely soon be present all around us in composites, sensors, batteries, electronics, and optoelectronics, if the technology can be optimized to a sufficient degree. Optical spectroscopies, and in particular nanospectroscopy, play an integral role in 2D material development and characterization, as well as in the novel device analysis. For example, Raman spectroscopy allows us to quickly, easily, and precisely characterize the obtained samples in terms of layer thickness, doping, impurities, defects, etc. In addition, TERS results demonstrate nanoscale detection of structural defects in 2D materials and offer detailed information on inhomogeneities as well as the local chemical composition of the material through the presence, possible shifts or splittings, and linewidths of the observed Raman peaks. PL spectroscopy allows confirming or excluding the presence of impurities or adsorbents in 2D materials and studying their electronic structure. As a result, the characterization data give us more details on the success or limitations of different synthesis methods, which we can use to improve the synthesis methods and device performance. Lots of commercial products based on graphene have already been developed and are available to purchase, while other devices based on the discussed 2D materials have great potential to be introduced in the near future, so we might see them on the market soon.

Bibliography

[1] Nicolosi V, Chhowalla M, Kanatzidis MG, Strano MS, Coleman JN. Liquid exfoliation of layered materials. Science. 2013;340:1226419.

[2] Madkour LH. Carbon nanomaterials and two-dimensional transition metal dichalcogenides (2D TMDCs). Nanoelectron Mater. 2019;165–245.

[3] Celasco E, Chaika AN, Stauber T, Zhang M, Ozkan C, Ozkan C, Ozkan U, Palys B, Harun SW, editors. Handbook of Graphene Set, I-VIII. Scrivener Publishing LLC, Wiley; 2019. p. 375–500.

[4] Di Bartolomeo A. Emerging 2D materials and their Van Der Waals Heterostructures. Nanomater (Basel). 2020:10.

[5] Miró P, Audiffred M, Heine T. An atlas of two-dimensional materials. Chem Soc Rev. 2014;43(18):6537.

[6] Kaul AB. Two-dimensional layered materials: structure, properties, and prospects for device applications. J Mater Res. 2014;29(3):348–61.

[7] Chacko L, Swetha AK, Anjana R, Jayaraj MK, Aneesh PM. Wasp-waisted magnetism in hydrothermally grown MoS_2 nanoflakes. Mater Res Express. 2016;3(11):116102.

[8] Vogel EM, Robinson JA. Two-dimensional layered transition-metal dichalcogenides for versatile properties and applications. Mater Res Soc Bull. 2015;40:558–63.

[9] Gablech I et al. Monoelemental 2D materials-based field effect transistors for sensing and biosensing: phosphorene, antimonene, arsenene, silicene, and germanene go beyond graphene. Trends Anal Chem. 2018;105:251–62.
[10] Vogt P, De Padova P, Quaresima C, Avila J, Frantzeskakis E, Asensio MC, Resta A, Ealet B, Lay GL. Silicene: compelling experimental evidence for graphenelike two-dimensional silicon. Phys Rev Lett. 2012;108(15):155501.
[11] Chatterjee B. Wonder material of 21st Century, Part 1: Development of graphene – a unique material, 1–8, 2021.
[12] Novoselov KS, Geim AK, Morozov SV, Jiang D, Zhang Y, Dubonos SV et al. Electric field effect in atomically thin carbon films. Science. 2004;306:666–9.
[13] Novoselov KS, Fal'ko VI, Colombo L, Gellert PR, Schwab MG, Kim K. A roadmap for graphene. Nature. 2012;192–200.
[14] Geim AK. Graphene: status and prospects. Science. 2009;324(5934):1530–4.
[15] Roman RE, Pugno NM, Cranford SW. Mechanical characterization of 2D nanomaterials and composites. In: Silvestre N, editor. Advanced Computational Nanomechanics. 2016. p. 201–42.
[16] Liang L, Zhang J, Sumpter BG, Tan Q, Tan P-H, Meunier V. Low-frequency shear and layer-breathing modes in Raman scattering of two-dimensional materials. ACS Nano. 2017;11(12):11777–802.
[17] Wang QH, Kalantar-Zadeh K, Kis A, Coleman JN, Strano MS. Electronics and optoelectronics of two-dimensional transition metal dichalcogenides. Nat Nanotechnol. 2012;7:699–712.
[18] Novoselov KS. Nobel lecture: graphene: materials in the flatland. Rev Mod Phys. 2011;83:837–49.
[19] Soldano C, Mahmood A, Dujardin E. Production, properties and potential of graphene. Carbon. 2010;48:2127–50.
[20] Peigney A, Laurent C, Flahaut E, Bacsa RR, Rousset A. Specific surface area of carbon nanotubes and bundles of carbon nanotubes. Carbon. 2001;39:507–14.
[21] Castro Neto AH, Guinea F, Peres NMR, Novoselov KS, Geim AK. The electronic properties of graphene. Rev Mod Phys. 2009;81:109–62.
[22] Hulman M. Raman spectroscopy of graphene. In: Graphene: Properties, Preparation, Characterisation and Applications, Woodhead Publishing Series in Electronic and Optical Materials. 2021. p. 381–411.
[23] Electronic properties of graphene probed at the nanoscale (Chapter 14). In: Mikhailov S, editor. Physics and Applications of Graphene – Experiments. 2011. p. 353–78. https://doi.org/10.5772/590.
[24] Gupta A, Sakthivel T, Seal S. Recent development in 2D materials beyond graphene. Prog Mater Sci. 2015;73:44–126.
[25] Wallace PR. Erratum: the band theory of graphite. Phys Rev. 1947;71(622):258.
[26] Dubois SM-M, Zanolli Z, Declerck X, Charlier J-C. Electronic properties and quantum transport in graphene-based nanostructures. Eur Phys J B. 2009;72:1–24.
[27] Nine MJ, Cole MA, Tran DNH, Losic D. Graphene: a multipurpose material for protective coatings. J Mater Chem A Mater Energy Sustain. 2015;3:12580–602.
[28] Avouris P. Graphene: electronic and photonic properties and devices. Nano Lett. 2010;10:4285–94.
[29] Mayorov AS, Gorbachev RV, Morozov SV, Britnell L, Jalil R, Ponomarenko LA et al. Micrometer-scale ballistic transport in encapsulated graphene at room temperature. Nano Lett. 2011:2396–9.
[30] Balandin AA, Ghosh S, Bao W, Calizo I, Teweldebrhan D, Miao F et al. Superior thermal conductivity of single-layer graphene. Nano Lett. 2008;8:902–7.

[31] Kim SJ, Choi K, Lee B, Kim Y, Hong BH. Materials for flexible, stretchable electronics: graphene and 2D materials. Annu Rev Mater Res. 2015;45(1):63–84.
[32] Fonash S, Van de Voorde M. Engineering, Medicine and Science at the Nano-Scale. 2018. 296p.
[33] Radadiya TM. A properties of graphene. Eur J Mater Sci. 2015;2(1):6–18.
[34] Park I-J, Kim TI, Yoon T, Kang S, Cho H, Cho NS et al. Flexible and transparent graphene electrode architecture with selective defect decoration for organic light-emitting diodes. Adv Funct Mater. 2018;28:1704435.
[35] Wang J, Liang M, Fang Y, Qiu T, Zhang J, Zhi L. Rod-coating: towards large-area fabrication of uniform reduced graphene oxide films for flexible touch screens. Adv Mater. 2012;24:2874–8.
[36] Xia K, Wu W, Zhu M, Shen X, Yin Z, Wang H et al. CVD growth of perovskite/graphene films for high-performance flexible image sensor. Sci Bull (Beijing). 2020;65:343–9.
[37] Kim H, Park K-Y, Hong J, Kang K. All-graphene-battery: bridging the gap between supercapacitors and lithium ion batteries. Sci Rep. 2014;4:5278.
[38] Kostarelos K, Vincent M, Hebert C, Garrido JA. Graphene in the design and engineering of next-generation neural interfaces. Adv Mater. 2017;29.
[39] Hong J-Y, Sohn E-H, Park S, Park HS. Highly-efficient and recyclable oil absorbing performance of functionalized graphene aerogel. Chem Eng J. 2015;269:229–35.
[40] Piper JR, Fan S. Broadband absorption enhancement in solar cells with an atomically thin active layer. ACS Photonics. 2016;3(4):571–7.
[41] Mao J, Wang Y, Zheng Z, Deng D. The rise of two-dimensional MoS_2 for catalysis. Front Phys. 2018;13.
[42] Tsai M-Y, Tarasov A, Hesabi ZR, Taghinejad H, Campbell PM, Joiner CA et al. Flexible MoS_2 field-effect transistors for gate-tunable piezoresistive strain sensors. ACS Appl Mater Interfaces. 2015;7:12850–5.
[43] Kloprogge JT, Ponce CP, Loomis TA. The Periodic Table: Nature's Building Blocks: An Introduction to the Naturally Occurring Elements, Their Origins and Their Uses. Elsevier; 2021. p. 633–883.
[44] Hao G, Kou L, Lu D, Peng J, Li J, Tang C, Zhong J. Electrostatic properties of two-dimensional WSe2 nanostructures. J Appl Phys. 2016;119(3):035301.
[45] Fang H, Chuang S, Chang TC, Takei K, Takahashi T, Javey A. High-performance single layered WSe_2 p-FETs with chemically doped contacts. Nano Lett. 2012;12:3788–92.
[46] Wang J, Ma F, Liang W, Wang R, Sun M. Optical, photonic and optoelectronic properties of graphene, h-BN and their hybrid materials. Nanophotonics. 2017;6:943–76.
[47] Ko PJ, Abderrahmane A, Takamura T, Kim N-H, Sandhu A. Thickness dependence on the optoelectronic properties of multilayered GaSe based photodetector. Nanotechnology. 2016;27:325202.
[48] Shmavonyan GSh, Vázquez-Vázquez C, López-Quintela MA. Single-step rubbing method for mass production of large-size and defect-free 2D materials. Transl Mater Res. 2017;4:025001.
[49] Novoselov KS, Jiang D, Schedin F, Booth TJ, Khotkevich VV, Morozov SV et al. Two-dimensional atomic crystals. Proc Natl Acad Sci USA. 2005;102:10451–3.
[50] Jayasena B, Subbiah S. A novel mechanical cleavage method for synthesizing few-layer graphenes. Nanoscale Res Lett. 2011;6:95.
[51] Lotya M, King PJ, Khan U, De S, Coleman JN. High-concentration, surfactant-stabilized graphene dispersions. ACS Nano. 2010;4:3155–62.
[52] Hernandez Y, Nicolosi V, Lotya M, Blighe FM, Sun Z, De S et al. High-yield production of graphene by liquid-phase exfoliation of graphite. Nat Nanotechnol. 2008;3:563–8.
[53] Park S, Ruoff RS. Chemical methods for the production of graphenes. Nat Nanotechnol. 2009;4:217–24.

[54] Hofmann M, Chiang W-Y, Nguyễn TD, Hsieh Y-P. Controlling the properties of graphene produced by electrochemical exfoliation. Nanotechnology. 2015;26:335607.
[55] Zhu Y, Murali S, Stoller MD, Velamakanni A, Piner RD, Ruoff RS. Microwave assisted exfoliation and reduction of graphite oxide for ultracapacitors. Carbon. 2010;48:2118–22.
[56] Li X, Cai W, An J, Kim S, Nah J, Yang D et al. Large-area synthesis of high-quality and uniform graphene films on copper foils. Science. 2009;324:1312–4.
[57] Chae SJ, Güneş F, Kim KK, Kim ES, Han GH, Kim SM et al. Synthesis of large-area graphene layers on poly-nickel substrate by chemical vapor deposition: wrinkle formation. Adv Mater. 2009;21:2328–33.
[58] Emtsev KV, Bostwick A, Horn K, Jobst J, Kellogg GL, Ley L et al. Towards wafer-size graphene layers by atmospheric pressure graphitization of silicon carbide. Nat Mater. 2009;8:203–7.
[59] Keith E, Whitener JR, Sheehan PE. Graphene synthesis. Diam Relat Mater. 2014;46:25–34.
[60] Schwierz F, editor. Two-Dimensional Electronics – Prospects and Challenges. Printed Edition of the Special Issue Published in Electronics. MDPI AG; 2016. p. 1–250.
[61] Moreau E, Ferrer FJ, Vignaud D, Godey S, Wallart X. Graphene growth by molecular beam epitaxy using a solid carbon source. Phys Status Solidi. 2010;207:300–3.
[62] Hernández-Rodríguez I, García JM, Martín-Gago JA, de Andrés PL, Méndez J. Graphene growth on Pt(111) and Au(111) using a MBE carbon solid-source. Diam Relat Mater. 2015;57:58–62.
[63] Janowska I, Vigneron F, Bégin D, Ersen O, Bernhardt P, Romero T et al. Mechanical thinning to make few-layer graphene from pencil lead. Carbon. 2012;50:3106–10.
[64] Paton KR, Varrla E, Backes C, Smith RJ, Khan U, O'Neill A et al. Scalable production of large quantities of defect-free few-layer graphene by shear exfoliation in liquids. Nat Mater. 2014;13:624–30.
[65] Liu X, Zheng M, Xiao K, Xiao Y, He C, Dong H et al. Simple, green and high-yield production of single- or few-layer graphene by hydrothermal exfoliation of graphite. Nanoscale. 2014;6:4598–603.
[66] Zhao W, Fang M, Wu F, Wu H, Wang L, Chen G. Preparation of graphene by exfoliation of graphite using wet ball milling. J Mater Chem. 2010;20:5817–9.
[67] Bae S, Kim H, Lee Y, Xu X, Park J-S, Zheng Y et al. Roll-to-roll production of 30-inch graphene films for transparent electrodes. Nat Nanotechnol. 2010;5:574–8.
[68] Subrahmanyam KS, Panchakarla LS, Govindaraj A, Rao CNR. Simple method of preparing graphene flakes by an arc-discharge method. J Phys Chem C Nanomater Interfaces. 2009;113:4257–9.
[69] Haigh SJ, Gholinia A, Jalil R, Romani S, Britnell L, Elias DC et al. Cross-sectional imaging of individual layers and buried interfaces of graphene-based heterostructures and superlattices. Nat Mater. 2012;11:764–7.
[70] Pan D, Zhang J, Li Z, Wu M. Hydrothermal route for cutting graphene sheets into blue-luminescent graphene quantum dots. Adv Mater. 2010;22:734–8.
[71] López-Quintela MA, Shmavonyan GSh, Vázquez Vázquez C. Method for producing sheets for graphene, Patent No: ES2575711 B2, November 3, 2016. EP3246286 A1.
[72] López-Quintela MA, Shmavonyan GSh, Vázquez Vázquez C. Method for producing sheets of graphene, USPTO patent US 10,968,104 B2, April 6, 2021.
[73] Shmavonyan G. Unique nanostripes and sheets of 2D atomic materials obtained by substrates rubbing technology. In: The 8th Annual International Conference on Chemistry, July 20–23, 2020, Athens, Greece.
[74] Shmavonyan G, Vázquez-Vázquez C, López-Quintela MA. Technology for mass production of 2D atomic materials. In: EuroSciCon Conference on Graphene and Carbon Nanotechnology, Nanoscience and Graphene Nanotechnology, November 25–27, 2019, Tokyo, Japan.
[75] Shmavonyan GSh, Mailian A, Mailian R. Anisotropy of carrier mobility in multilayered graphite structures obtained by rubbing. In: The 10^{th} International Conference on Nanosciences and Nanotechnologies, July 9–12, 2013, Thessaloniki, Greece.

[76] Shmavonyan GSh, Mailian AR, Mailyan MR, López-Quintela MA. Obtaining graphene on paper from pencil drawn lines. European Conference on the Synthesis, Characterization and Applications of Graphene, February 18–21, 2014, Lanzarote, Canary Island, Spain.
[77] Wang X, You H, Liu F, Li M, Wan L, Li S et al. Large-scale synthesis of few-layered graphene using CVD. Chem Vap Depos. 2009;15:53–6.
[78] Geim AK, Novoselov KS. The rise of graphene. Nat Mater. 2007183–91.
[79] Bhuyan MSA, Uddin MN, Islam MM, Bipasha FA, Hossain SS. Synthesis of graphene. Int Nano Lett. 2016;6:65–83.
[80] Zhao Q, Puebla S, Zhang W, Wang T, Frisenda R, Castellanos-Gomez A. Thickness identification of thin InSe by optical microscopy methods. Adv Photon Res. 2020;1:2000025.
[81] Wang YY et al. Thickness identification of two-dimensional materials by optical imaging. Nanotechnology. 2012;23:495713.
[82] Han B. Deep-learning-enabled fast optical identification and characterization of 2D materials. Adv Mater. 2020;32(29):2000953.
[83] Butler SZ, Hollen SM, Cao L, Cui Y et al. Progress, challenges, and opportunities in two-dimensional materials beyond graphene. ACS Nano. 2013;7(4):2898–926.
[84] Shmavonyan GS, Sevoyan GG, Aroutiounian VM. Enlarging the surface area of monolayer graphene synthesized by mechanical exfoliation. Armen J Phys. 2013;6:1–6.
[85] Koh YK. Heat transport by phonons in crystalline materials and nanostructures. Ph.D. Thesis. University of Illinois at Urbana-Champaign; 2010.
[86] Basko DM. New J Phys. 2009;11:095011.
[87] Hasan T et al. Nanotube and graphene polymer composites for photonics and optoelectronics. In: Hayden O, Nielsch K, editors. Molecular- and Nano-Tubes. Boston, MA: Springer; 2011.
[88] Javed H, Pani S, Antony J, Sakthivel M, Drillet J-F. Synthesis of mesoporous carbon spheres via a soft-template route for catalyst supports in PEMFC cathodes. Soft Matter. 2021;17:7743–54.
[89] Zhang Y-L, Guo L, Xia H, Chen Q-D, Feng J, Sun H-B. Photoreduction of graphene oxides: methods, properties, and applications. Adv Opt Mater. 2014;2(1):10–28.
[90] Peña-Álvarez M, del Corro E, Baonza VG, Taravillo M. Probing the stress effect on the electronic structure of graphite by resonant Raman spectroscopy. J Phys Chem C. 2014;118(43):25132–40.
[91] Beyssac O, Lazzeri M. Application of Raman spectroscopy to the study of graphitic carbons in the Earth sciences. EMU Notes Mineral. 2012;12(1):415–54.
[92] Kuila T, Bose S, Mishra AK, Khanra P, Kim NH, Lee JH. Chemical functionalization of graphene and its applications. Prog Mater Sci. 2012;57(7):1061–105.
[93] Kuila T, Sheng Y, Murmu NC. Graphene/conjugated polymer nanocomposites for optoelectronic and biological applications. In: Fundamentals of Conjugated Polymer Blends, Copolymers and Composites: Synthesis, Properties and Applications. 2015. p. 229–79.
[94] Shvets V. Polymer masks for nanostructuring of graphene. PhD Thesis. DTU Nanotech; 2015.
[95] Bruna M, Ott AK, Ijäs M, Yoon D, Sassi U, Ferrari AC. Doping dependence of the Raman spectrum of defected graphene. ACS Nano. 2014;8:7432–41.
[96] Gadelha AC, Vasconcelos TL, Cançado LG, Jorio A. Nano-optical imaging of in-plane homojunctions in graphene and MoS_2 van der Waals heterostructures on Talc and SiO_2. J Phys Chem Lett. 2021:7625–31.
[97] Malard L, Lafetá L, Cunha R, Nadas R, Gadelha A, Cancado G, Jorio A. Studying 2D materials with advanced Raman spectroscopy: CARS, SRS and TERS. Phys Chem Chem Phys. 2021;23:23428–44.
[98] Lee J, Crampton KT, Tallarida N, Apkarian VA. Visualizing vibrational normal modes of a single molecule with atomically confined light. Nature. 2019;568:78–82.
[99] Li H, Zhang Q, Yap CCR, Tay BK, Edwin THT, Olivier A, Baillargeat D. From bulk to monolayer MoS2: evolution of Raman scattering. Adv Funct Mater. 2012;22(7):1385–90.

[100] Lee C, Yan H, Brus LE, Heinz TF, Hone J, Ryu S. Anomalous lattice vibrations of single- and few-layer MoS_2. ACS Nano. 2010;4:2695–700.
[101] Lee J-U, Kim M, Cheong H. Raman spectroscopic studies on two-dimensional materials. Appl Microsc. 2015;45(3):126–30.
[102] Zhang X, Han WP, Wu JB, Milana S, Lu Y, Li QQ et al. Raman spectroscopy of shear and layer breathing modes in multilayer MoS_2. Phys Rev B, Condens Matter Mater Phys. 2013;87.
[103] Rodriguez RD, Müller S, Sheremet E, Zahn DRT, Villabona A, Lopez-Rivera SA et al. Selective Raman modes and strong photoluminescence of gallium selenide flakes on sp2 carbon. J Vac Sci Technol, B Nanotechnol Microelectron: Materials, Processing, Measurement, Phenomena. 2014:04E106.
[104] Wu Q, Tagani MB, Zhang L, Wang J, Xia Y et al. Electronic tuning in WSe_2/Au via van der Waals interface twisting and intercalation. ACS Nano. 2022;16(4):6541–51.
[105] Iqbal MW, Shahzad K, Akbar R, Hussain G. A review on Raman finger prints of doping and strain effect in TMDCs. Microelectron Eng. 2020:111152.
[106] Chakraborty B, Bera A, Muthu DVS, Bhowmick S, Waghmare UV, Sood AK. Symmetry-dependent phonon renormalization in monolayer MoS_2 transistor. Phys Rev B. 2012.
[107] Khalil HMW, Khan MF, Eom J, Noh H. Highly stable and tunable chemical doping of multilayer WS_2 field effect transistor: reduction in contact resistance. ACS Appl Mater Interfaces. 2015;7:23589–96.
[108] Peimyoo N, Yang W, Shang J, Shen X, Wang Y, Yu T. Chemically driven tunable light emission of charged and neutral excitons in monolayer WS_2. ACS Nano. 2014;8:11320–9.
[109] Özden A, Şar H, Yeltik A, Madenoğlu B, Sevik C, Ay F et al. CVD grown 2D MoS_2 layers: a photoluminescence and fluorescence lifetime imaging study. Phys Status Solidi RRL. 2016;10:792–6.
[110] Xu L, Zhao L, Wang Y, Zou M, Zhang Q, Cao A. Analysis of photoluminescence behavior of high-quality single-layer MoS_2. Nano Res. 2019;12:1619–24.
[111] Su W, Roy D. Visualizing graphene edges using tip-enhanced Raman spectroscopy. J Vac Sci Technol, B Nanotechnol Microelectron. 2013;31:041808.
[112] Kato R, Umakoshi T, Sam RT, Verma P. Probing nanoscale defects and wrinkles in MoS_2 by tip-enhanced Raman spectroscopic imaging. Appl Phys Lett. 2019;114:073105.
[113] Smithe KKH, Krayev AV, Bailey CS, Lee HR, Yalon E, Aslan ÖB et al. Nanoscale heterogeneities in monolayer $MoSe_2$ revealed by correlated scanning probe microscopy and tip-enhanced Raman spectroscopy. ACS Appl Nano Mater. 2018;1:572–9.
[114] Jit S, Das S, editors. 2D Nanoscale Heterostructured Materials – Synthesis, Properties, and Applications. Elsevier; 2020. https://www.elsevier.com/books/2d-nanoscale-heterostructured-materials/jit/978-0-12-817678-8.
[115] The Nobel Prize in Physics 2000. NobelPrize.org. Nobel Prize Outreach AB 2022. Sun. 17 Jul 2022.
[116] Zhang T, Fu L. Controllable chemical vapor deposition growth of two-dimensional heterostructures. Chem. 2018;4(4):671–89.
[117] Pant A, Mutlu Z, Wickramaratne D, Ca H, Lake RK, Ozkan CS, Tongay S. Fundamentals of lateral and vertical heterojunctions of atomically thin materials. Nanoscale. 2016;8:3870–87.
[118] Gao T, Song X, Du H et al. Temperature-triggered chemical switching growth of in-plane and vertically stacked graphene-boron nitride heterostructures. Nat Commun. 2015;6:6835.
[119] Novoselov KS, Mishchenko A, Carvalho A, Castro Neto AH. 2D materials and van der Waals heterostructures. Science. 2016;353:aac9439.
[120] Pospischil A, Furchi MM, Mueller T. Solar-energy conversion and light emission in an atomic monolayer p–n diode. Nat Nanotechnol. 2014;9:257–61.

[121] Fontana M, Deppe T, Boyd AK, Rinzan M, Liu AY, Paranjape M et al. Electron-hole transport and photovoltaic effect in gated MoS2 Schottky junctions. Sci Rep. 2013;3:1–6.
[122] Xu Z-Q, Zhang Y, Wang Z, Shen Y, Huang W, Xia X et al. Atomically thin lateral p–n junction photodetector with large effective detection area. 2D Mater. 2016041001.
[123] Moon JS, Seo H-C, Stratan F, Antcliffe M, Schmitz A, Ross RS et al. Lateral graphene heterostructure field-effect transistor. IEEE Electron Device Lett. 2013;34:1190–2.
[124] Wang H, Yu L, Lee Y-H, Shi Y, Hsu A, Chin ML et al. Integrated circuits based on bilayer MoS_2 transistors. Nano Lett. 2012;12:4674–80.
[125] Geim AK, Grigorieva IV. Van der Waals heterostructures. Nature. 2013;499:419–25.
[126] Kai N, Xiaocha W, Wenbo M. Spin-dependent electronic structure and magnetic anisotropy of two-dimensional SnO/Fe_4N heterostructures. J Phys Chem C. 2019. https://doi.org/acs.jpcc.9b06896.
[127] Yuan L, Ge J, Peng X, Zhang Q, Wu Z, Jian Y et al. A reliable way of mechanical exfoliation of large scale two dimensional materials with high quality. AIP Adv. 2016;6:125201.
[128] Kroemer H. Quasi-electric and quasi-magnetic fields in nonuniform semiconductors. RCA Rev. 1957;18:332–42.
[129] Hu X, Kou L, Sun L. Stacking orders induced direct band gap in bilayer $MoSe_2$-WSe_2 lateral heterostructures. Sci Rep. 2016;6:31122.
[130] Chen Y, Fan Z, Zhang Z, Niu W, Li C, Yang N et al. Two-dimensional metal nanomaterials: synthesis, properties, and applications. Chem Rev. 2018;118:6409–55.
[131] Xue Y, Zhang Y, Liu Y, Liu H, Song J, Sophia J et al. Scalable production of a few-layer MoS_2/WS_2 vertical heterojunction array and its application for photodetectors. ACS Nano. 2016;10:573–80.
[132] Xu H, Wu J, Feng Q, Mao N, Wang C, Zhang J. High responsivity and gate tunable graphene-MoS_2 hybrid phototransistor. Small. 2014;10:2300–6.
[133] Xiong XX, Kang J, Hu Q, Gu C, Gao T et al. Reconfigurable logic-in-memory and multilingual artificial synapses based on 2D heterostructures. Adv Funct Mater. 20201909645.
[134] Berry V. Impermeability of graphene and its applications. Carbon. 2013;62:1–10.
[135] Bernardo P, Drioli E. Membrane technology. In: Drioli E, Giorno L, Fontananova E, Editors-in-Chief. Comprehensive Membrane Science and Engineering. 2nd ed. Elsevier Science; 2017. p. 164–88.
[136] Cai X, Lai L, Shen Z, Lin J. Graphene and graphene-based composites as Li-ion battery electrode materials and their application in full cells. J Mater Chem A Mater Energy Sustain. 2017;5:15423–46.
[137] Son IH, Park JH, Park S, Park K, Han S, Shin J et al. Graphene balls for lithium rechargeable batteries with fast charging and high volumetric energy densities. Nat Commun. 2017;8:1561.
[138] Acik M, Darling SB. Graphene in Perovskite solar cells: device design, characterization and implementation. J Mater Chem A Mater Energy Sustain. 2016;4(17):6185–235.
[139] Justino CIL, Gomes AR, Freitas AC, Duarte AC, Rocha-Santos TAP. Graphene based sensors and biosensors. Trends Analyt Chem. 2017;91:53–66.
[140] Warnke PH. Orthopaedic tissue engineering. In: Sivananthan S, Sherry E, Warnke P, Miller M, editors. Mercer's Textbook of Orthopaedics and Trauma. Tenth edition. London: CRC Press; 2012.
[141] Nguyen D, Valet M, Dégardin J, Boucherit L, Illa X, de la Cruz J et al. Novel graphene electrode for retinal implants: an biocompatibility study. Front Neurosci. 2021;15:615256.
[142] Kim K, Choi J-Y, Kim T, Cho S-H, Chung H-J. A role for graphene in silicon-based semiconductor devices. Nature. 2011;479:338–44.
[143] Lin Y-M, Jenkins KA, Valdes-Garcia A, Small JP, Farmer DB, Avouris P. Operation of graphene transistors at gigahertz frequencies. Nano Lett. 2009;9:422–6.

[144] Nourbakhsh A, Zubair A, Sajjad RN, Tavakkoli KGA, Chen W, Fang S et al. MoS_2 field-effect transistor with sub-10 nm channel length. Nano Lett. 2016;16:7798–806.
[145] Lin Y-M, Valdes-Garcia A, Han S-J, Farmer DB, Meric I, Sun Y et al. Wafer-scale graphene integrated circuit. Science. 2011;332:1294–7.
[146] Liu H, Neal AT, Ye PD. Channel length scaling of MoS_2 MOSFETs. ACS Nano. 2012;6:8563–9.
[147] Chahardeh JB. A review on graphene transistors. Int J Adv Res Comput Commun Eng. 2012;1.